Supplementary Materials for

Secreting and Sensing the Same Molecule Allows Cells to Achieve Versatile Social Behaviors

Hyun Youk and Wendell A. Lim*

*Corresponding author. E-mail: lim@cmp.ucsf.edu

Published 7 February 2014, *Science* **343**, 1242782 (2014)
DOI: 10.1126/science.1242782

The PDF file includes:

Materials and Methods

Strain background and construction

The yeast strains that we used in our study are listed at the end of this supplementary material (table S1). Unless stated otherwise, the main genotype of the parent yeast strain for all our secrete-and-sense and sense-only strains was *MATα far1Δ bar1Δ*. Deletion of the *FAR1* gene ensured that our cells could sense the α-factor without arresting their growth. Where necessary, we knocked out the genes in the yeast through the standard PCR-mediated gene deletion method. We performed all yeast transformations through the standard lithium acetate method. Our basic cloning method relied on a set of integrating plasmids (pNH603, pNH604, pNH605, pSV606, pJW607, pJW608) that contained multiple restriction digest sites and integrated as a single copy into the yeast being transformed. Multiple cloning sites enabled insertion of a yeast promoter and an ORF whose expression is controlled by the promoter. All ORFs in these expression plasmids are followed by the *Candida albicans* Adh1 transcriptional terminator. The plasmids - pNH603, pNH604, pNH605, and pSV606 - contained auxotrophic complementation markers from *Candida albicans* or *Candida glabrata*. pJW607 and pJW608 contained markers that conferred transformed yeast resistance to the antibiotics G418 (through *kanMX*) and hygromycin B (through '*HygB*' resistance marker). Each plasmid also had approximately 500-bp sequences that were homologous to the 5' and 3' regions up and downstream of the corresponding auxotrophic locus in the yeast that the plasmid was to be inserted into. Details of these plasmids are given in table S2.

Fluorescence measurements

Single-cell fluorescence was measured using a Becton Dickinson LSRII (Custom-made) flow cytometer with a robotic arm for handling samples in a 96-well plate. The average single-cell GFP fluorescence due to the fluorescent proteins in individual cells was measured using 488 nm excitation. Before measuring the mean single-cell fluorescence using this flow cytometer, all yeast cells were grown using the protocol outlined in 'culture growth' section. α-factor responding cells expressed α-inducible GFP in our experiments. At each time point, α-factor responsive cells were gated and their mean fluorescence was binned by cell size using FSC and SSC distributions. For bimodal population of fluorescent cells, same size-normalization was used for both groups of cells, ensuring equal comparisons between differing cell sizes. In our co-cultures of a sense-only strain with a secrete-and-sense strain we gated the secrete and sense cells that are pheromone responsive separately from the sense-only cells. Both were normalized to equal volumes by using the FSC and SSC distributions observed in FACS. . For both dose response and time-course experiments, unless otherwise stated, sample aliquots were treated with 5 μg/ml cycloheximide (Sigma-Aldrich) before measuring single-cell fluorescence using our flow cytometer.

Culture growth

We used standard synthetic media with various concentrations of doxycycline in our experiments. Cells were cultured at 30C as 5mL batch cultures in rotating glass tubes at a fixed rotation frequency. As our model shows, different geometries of tubes, growth wells and shaking conditions affect the local concentration of the α-factor and can qualitatively change the resulting dynamics. Thus our results are sensitive to culturing conditions. At each time point, we subsampled an aliquot from the culture for flow

cytometry that yielded the Kolmogorov mixing length scale as computed in our mathematical model (see section on our mathematical model). By measuring the Optical Density (OD_{600}: Absorbance at 600nm), we obtained the relative population sizes per culture. In co-culture experiments with the basic secrete and sense and sense only strains, each strain was pre-incubated by itself, such that each strain was in a log-phase growth, they were mixed as co-cultures.

Supplementary Text

Description of phenomenological model

To complement our experimental findings, we devised a minimal phenomenological model in an attempt to explain the main features of our experiments. As we will explain below, our simplified model has many limitations and a more detailed realistic model will likely better capture all the features of our experimental work. But our goal here was to devise a simple toy model that captured the main qualitative essence of our key experimental results and provide qualitative intuition rather than attempt to fit every feature of our experiments in detail.

Insightful previous studies, such as Rappaport and Barkai (*53*), Jin *et al.* (*54*), Barkai *et al.* (*52*), A. Pai *et al.* (*32*), Mehta *et al.* (*30*) and Danino *et al.* (*34*), Shvartsman *et* al. (*72*), and T. Long *et al.* (*69*), to name just a few, all have provided detailed, very insightful and elegant mathematical models that have together revealed the design principles underlying the yeast's mating-efficiency (using both the α-factor and the Bar1 protease), bacteria's ability to integrate various quorum-sensing signals, and metazoan autocrine signaling. Motivated by these detailed studies, below we provide a simple model to explain: (a) Self-communication due to the local concentration of the α-factor surrounding a secrete-and-sense cell (b) Neighbor-communication (intercellular communication) due to the global concentration of the α-factor, (c) How changing the receptor abundance and the secretion rate can tune self-communication and neighbor-communication, and (d) Interplay between self- and neighbor-communication when positive feedback and the Bar1 protease are present. We will obtain many of our model's parameters from our experiments as well as from previous models of the mating pathway (*52-54*).

Intuitive summary of our model

Here we provide an intuitive summary of the calculations that we perform in the subsequent sections. A cell that is constantly secreting a molecule builds a diffusion gradient of that molecule around itself. This is true for both non-agitated and rotating liquid cultures. In rotating liquid cultures such as the ones that we used in our experiments, the diffusion profile of the molecules does not continue undisturbed out to an arbitrarily long distance away from the secreting cell. Instead, convection of the fluid disturbs the tail-end of the diffusion profile (i.e., far from the cell) and causes mixing of the molecules at a distance above the characteristic length scale called the 'Kolmogorov mixing length scale' that we compute in the next section. The key point here is that even when the liquid culture is being agitated as in our experiments, the secreted molecules do not get 'well-mixed' down to an arbitrarily small length scale. Thus a cloud of the

secreted molecules can form around the secrete-and-sense cell in a “mixing” liquid culture. The physics that is responsible for this mixing length scale is analogous to the one that prevents the liquid culture of cells inside a small well (e.g., wells of the standard 96-well plate) from being well-mixed when the well is shaken/agitated by a large flat-bed shaker that is typically used for rotatory mixing large flasks of liquid cultures (i.e., trying to rotationally agitate 96-wells of cells with a flat-bed shaker that is typically used for mixing 5L flasks). The cells within the small well do not mix well. Instead, the cells sediment at the bottom of the well because the radius of the circular motion of the shaker is too large compared to the dimensions of the well (i.e., cells in the 96-well plate sediment and do not get agitated in the large-radius flat-bed shaker).

The secrete-and-sense cell senses the local cloud (i.e., 'local concentration') of the α-factor, which forms very quickly (evidenced by both our experiments and calculations below). This sensing is what we call 'self-communication' (note that this local cloud would still exist in non-agitated, stationary cells by default). Importantly, this local concentration cannot increase up to infinity because it is depleted by diffusion. Instead it saturates at a level that is proportional to the secretion rate (and inversely proportional to the diffusion constant), leading to the saturation in the pFUS1-GFP level in the self-communicating secrete-and-sense cells as seen in our experiments (e.g., Fig. 2C - left panel) and calculations (section 1 below). The sense-only cells do not have such a local cloud of the α-factor since they do not secrete any α-factor. Instead, in our cultures, the sense-only cells sense the global concentration of the α-factor that is contributed by all the secrete-and-sense cells. In particular, the tail of the α-factor diffusion profile from each secrete-and-sense cell is all mixed together by convection, yielding the global concentration of the α-factor sensed by the sense-only cells. Our calculations show that the discrepancy between the local and global concentrations can be quite large, which is also consistent with the measured GFP differences between the secrete-and-sense and the sense-only cells in our experiments. Note that GFP is the most direct way to measure the α-factor concentration differences because we cannot measure it by other methods due to the nature of the microenvironments (i.e., other methods would disturb / cannot access the microenvironment of the cells). The high sensitivity of the pFUS1-GFP expression to small changes in the α-factor concentration (as shown in fig. S1) makes GFP a sensitive probe for both local and global concentrations of the α-factor in our experiments.

When the density of secrete-and-sense cells (OD) is high, the global concentration of the α-factor is larger than the local concentration around each secrete-and-sense cell (since the local concentration is capped at a finite level that is proportional to the secretion rate whereas the global concentration can grow without an upper bound). This leads to the sense-only and secrete-and-sense cells both sensing the same amount of the α-factor (the global concentration) in the high-density cultures in our experiments. When the cell density is low, both our model and experiments show that the local concentration is larger than the global concentration. Intuitively, we can understand this by noticing that the number of the α-factor molecules within the microenvironment of the secrete-and-sense cell determines the local concentration. But the global concentration depends on the macroscopic volume of the media (~5 mL in our experiments). Thus an increase of a few α-factor molecules in the microenvironment can lead to a significant increase in the local concentration (due to microscopic volume) whereas it is insignificant in changing the global concentration (due to the macroscopic volume).

In the following sections, we will make the above qualitative descriptions concrete through a mathematical model that provides qualitative insights into the main features of our experiments.

1. Self-communication due to the local concentration of the α-factor that surrounds the secrete-and-sense cell

In this section, we will compute the Kolmogorov mixing length scale. This is one of several length scales in theories of fluid dynamics that estimates the typical length scale over which the local concentration of the α-factor can be maintained around a cell. We will also compute the pFUS1-GFP temporal response dynamics in the self-communicating secrete-and-sense cell.

Even within a liquid culture that is constantly being agitated, a cell that secretes molecules can create a local concentration gradient around itself due to length scales in which laminar flow can be maintained, below regions of turbulence. The is characterized by the 'Kolmogorov mixing length scale' - a fundamental feature of fluid dynamics. It characterizes the length-scale below which a laminar flow (and gradient of secreted molecules) can be maintained, and above which the turbulent flow within the mixing culture creates a well-mixed environment. Previous studies have experimentally demonstrated that a local concentration around a cell can be maintained in a liquid culture (e.g., the hydrolysis of sucrose into glucose and fructose by invertase just outside the cell in a rotatory liquid culture creates a local concentration of the monosaccharaides around the cell) (*86*). Specifically, the Kolmogorov length scale η is given by: $\eta = (\nu^3/\varepsilon)^{1/4}$, where ε is the energy dissipation rate (characterizing energy loss from eddy currents), and ν is the kinematic viscosity. The value for ε is usually determined empirically, which makes computing the exact value for η challenging. One can obtain a valid estimate of η by $\eta \sim L/(Re^{3/4})$, where *Re* is the Reynolds number of our rotatory cultures and *L* is the diameter of our culture tube (*99*). Using L = 2.4 cm and $Re \sim 3000$ (applies to our rotational cultures with a rotational frequency of 42 rounds/minute, dynamic viscosity of water at 30C of 0.798 N s/m^2, and density of water at 30C of 1000 kg/m^3) (*99*), we obtain $\eta \sim 60$ μm. Even using a relatively high $Re \sim 10000$, one still obtains $\eta \sim 30$ μm which is nearly 6 times the haploid yeast cell's average diameter (~5 μm) and is still enough for sustaining a local concentration of the secreted molecules around the cell. Hence these simple estimates indicate that the secrete-and-sense cells can maintain a local concentration gradient in our rotatory liquid culture.

To compare this length scale with the average distance between cells in our liquid cultures, we use that *OD*=1 corresponds to approximately 3x10^7 haploid yeast cells/mL. Hence at a very low density (OD=0.001), the average distance between two cells is approximately 320 μm. At a high cell density (OD=0.1), the cell-cell distance is approximately 70 μm (assuming that the cells are placed on cubic lattices). Hence all the cell densities that we used in our experiments yield average distances between the cells that are larger than the Kolmogorov length scale η. This means that neighbor-communication is due to a cell sensing the global pool of α-factor secreted by all the other cells in the culture (which we will compute using a 'mean-field' approximation in section 2), while self-communication is due to the secrete-and-sense cell sensing the local cloud of the α-factor that it has built around itself within the Kolmogorov length scale η.

We now compute the local concentration around a secrete-and-sense cell as a function time. Solving the diffusion equation in three spatial dimensions, with the initial condition that α-factor is absent everywhere, yields the concentration *c* over time *t* of α−factor at the surface of the secrete-and-sense cell with radius *R*:

$$c(R,t) = \frac{\sqrt{t}F_0}{\sqrt{\pi D}}\left\{1 - e^{\frac{-R^2}{Dt}} + \frac{R\sqrt{\pi}}{\sqrt{Dt}}erfc(\frac{R}{\sqrt{Dt}})\right\}, \qquad [\boldsymbol{S1}]$$

where *D* is the diffusion coefficient of the α-factor in water (D=150 mm^2/s, estimated by using the Stokes-Einstein relation and is similar to the value used by previous models of the mating pathway (*53, 54*)), and F_0 is the flux of the α−factor molecules secreted radially outward at the cell surface (in molecules/(area x time)). This is one of the solutions of the diffusion equation with a boundary condition that one can analytically obtain (*99, 100*). According to Eq. [S1], $c(R,t)$ increases in time until it reaches the concentration of $\frac{RF_0}{D}$, which is proportional to the secretion rate. The time scale for this increase is determined by the characteristic time for diffusion R^2/D, which is much faster than the time scale for transcription and translation. Specifically, the diffusion time scale is R^2/D = 20 ms (on the order of several milliseconds) while the time scale for the combined transcription-and-translation is on the order of several minutes. Therefore, we assume that the secrete-and-sense cell senses this constant, saturated level of the local concentration and expresses its GFP (through the pFUS1 promoter) in response to it.

Next we link the local concentration computed above (Eq. [S1]) with the pFUS1-GFP response in the secrete-and-sense cell. For all our strains with pFUS1-GFP (including the sense-only strains), the dynamics of the GFP production in the cell is given by

$$\frac{dG}{dt} = k([\alpha]) - \sigma G, \qquad [\boldsymbol{S2}]$$

where [α] is the concentration of the α−factor (local concentration for self-communication, global concentration for neighbor-communication), σ is the first order protein-degradation rate of GFP, *G* is the concentration of the GFP (protein), and $k([\alpha])$ is the net production rate (transcription and translation combined) of GFP per cell as a function of the concentration of the α-factor. The solution to Eq. [S2], with the initial condition that [α]=0, is

$$G([\alpha],t) = (G_0 - \frac{k([\alpha])}{\sigma})e^{-\sigma t} + \frac{k([\alpha])}{\sigma}\ , \qquad [\boldsymbol{S3}]$$

where G_0 is the basal level of the single-cell mean GFP fluorescence, assuming that GFP level is positively correlated with the fluorescence per cell. To make contact with our experimental data, we assume that the mean single-cell GFP fluorescence is directly proportional to *G*. Then without plugging any numbers into Eq. S3, we can see that for a fixed [α] (and thus fixed $k([\alpha])$, regardless of the functional form of *k*), $G([\alpha],t)$ increases over time and asymptotes to a constant level $k([\alpha])/\sigma$, mimicking the shape of the temporally increasing GFP levels of our basic secrete-sense strain (i.e., the secrete-and-sense strain with the endogenous STE2 promoter expressing Ste2) that we measured in our experiments (see Fig. 2C). Based on previous studies of our *FUS1* promoter (*51*), we let $k([\alpha])$ be a sigmoidal function of [α] and σ = ln(2)/T, where T is the doubling time of

our basic secrete-sense strain equal to 2.6 hrs, the maximum specific log-phase growth rate of basic secrete-and-sense strain obtained through Tecan plate reader and averaged over all our doxycycline concentrations. Our fit function k([α])/σ is shown in fig. S1. Using these values for each [doxycycline] that was used in Fig. 2B and fig. S4, we obtain the fit function G_{self}(t) shown in fig. S16 that describes the GFP level in the basic secrete-and-sense cells at a low total OD (OD=0.001) of the co-cultures in our experiment in which self-sensing is dominant. As fig. S16 shows, our model can explain the basic secrete-and-sense cell's response to self-sensing, represented by G_{self}(t). All the main features that we computed here apply to the other secrete-and-sense strains with different levels of Ste2. The only change, as we will see in section 3, is that the production function k([α]) will be different for different expression levels of Ste2 (fig. S9) because as shown in the circuit diagram (Fig. 2B), the receptor level directly affects the pFUS1 promoter that expresses GFP. We will compute the effect of changing the expression level of Ste2 receptor in section 3.

2. Neighbor-communication due to the global concentration of the α-factor

Having computed the basic secrete-and-sense strain's response to self-communication, our main goal in this section is to propose a simple model that captures the main trend in our data for the response of the basic sense-only strain (i.e., the sense-only strain with the endogenous promoter expressing Ste2) shown in fig. S4. We will show how changing the expression level of Ste2 changes the cell's response in section 3. The equation that describes the actual concentration of the α-factor that the sense-only cell feels is complicated due to many physical factors. For example, an exhaustive model would take into account how the distance between the cells are changing due to their random jostling motion within the rotatory liquid culture. There are also collisions between cells, which changes the time-average of the concentration of the α-factor sensed by the cell, that a more exhaustive model must take into account. Moreover the full model must take into account the effect of transition from the laminar to turbulent flow on the local concentration gradient around the secrete-and-sense cells, requiring analysis of the Navier-Stokes equation, which cannot be analytically solved for this transition. But at a low enough population density, in which the cells are sufficiently far apart from each other on average, as shown in our calculation of the average distance between cells in section 1, we can use the following phenomenological model that uses a 'mean-field' approach to computing the global concentration of the α-factor. We assume that the global concentration of the α-factor $\rho(t)$, on a length scale larger than the mixing length scale η, due to all the secrete-and-sense cells at time t is given by:

$$\frac{d\rho(t)}{dt} = rN_0e^{\mu t} - \gamma\rho(t)\,, \qquad [\boldsymbol{S4}]$$

where r is the secretion rate of the α-factor per cell (assumed to be constant, and depends only on the concentration of the doxycycline), μ is the specific growth rate of the secrete-and-sense strain, and γ is the first order degradation rate of the α-factor. Following the careful reasoning by Rappaport and Barkai (*53*) and Jin *et al* (*54*), we set γ=0.01 s^{-1}. For the initial condition $\rho(0)$=0, the solution to Eq. [S4] is

$$\rho(t) = \frac{rN_0}{\mu}(e^{\mu t} - e^{-\gamma t}) \qquad [\boldsymbol{S5}]$$

Eq. [S5] describes the global concentration of the α-factor, $\rho(t)$. Since the sensing of the global concentration of the α-factor triggers the signal transduction that involves the fast phosphorylation events (the mating pathway's MAPK signal-transduction) that are upstream of the much slower transcription/translation machineries, we assume that the production rate is $k(\rho(t))$ instead of introducing a time-delay between the change in $\rho(t)$ and sensing of the extracellular α-factor. Thus to obtain the mean single-cell GFP fluorescence of the sense-only strains over time, we use Eq. [S2], but now with $k(\rho(t))$ as the production rate of GFP:

$$\frac{dG_{others}}{dt} = k(\rho(t)) - \sigma G, \qquad [\boldsymbol{S6}]$$

where k is now an explicit function of time t.

To see how well Eq. [S6] describes the pure neighbor-communication (i.e., no self-communication), we first need to determine the values of r for each [doxycycline]. To do so, we note that there is a one-to-one correspondence between the pFUS1-GFP level and the concentration of the α-factor sensed by the cell (fig. S1). This is true for both secrete-and-sense and sense-only strains. Since we know the GFP level in the secrete-and-sense cells due to self-communication, we know the corresponding local concentration of the α-factor that surrounds the secrete-and-sense cells (through the one-to-one correspondence between GFP and [α] in fig. S1). Using this correspondence and Eq. [S1], we can compute the corresponding secretion flux F_0. Finally from this flux, we can compute the corresponding secretion rate (of secrete-and-sense cells in the co-cultures) through the following relationship:

$$r = 4\pi R^2 F_0\,, \qquad [\boldsymbol{S7}]$$

where R is the radius of the cell. We used R=2 μm as the radius of our haploid cells and we made the idealized assumption that this radius does not change during the lifetime of the cell (in reality, the cell's radius actually changes during cell cycle). Substituting the computed value of r into Eq. [S5] for each doxycycline concentration, then substituting the resulting $\rho(t)$ into Eq. [S6] and numerically solving the resulting Eq. [S6], we see how well our model (Eq. [S6]) describes the basic sense-only strains' GFP response for various secretion rates and ODs (see fits in fig. S17). More concretely, for each doxycycline concentration, our earlier fit of Eq. [3] to our data for the basic secrete-and-sense strain (fig. S16) yields $k([\alpha])/\sigma = c(R,\ t >> R^2/D)$. Then we use this value to solve for the flux F_0 via $c(R, t \gg \frac{R^2}{D}) = \frac{RF_0}{D}$ (result of Eq. [S1]). Then the total secretion rate per cell r is determined by Eq. [S7]. Doing so yields, for each value of [doxycycline], a value for r and a corresponding $\rho(t)$. For each value of [doxycycline], we use the corresponding $\rho(t)$ to numerically solve Eq. [S6], and compare the resulting solution (a curve in fig. S17) to our basic sense-only strain data (data points in fig. S17).

Note that there is no fit-parameter in Eq. [S6]. That is, we have fitted all the parameters in Eq. [S6] by using a different data set that pertains to the basic secrete-and-sense strain. We have not used any data for the basic sense-only strain to obtain any of the parameter values in Eq. [S6]. Thus solving Eq. [S6] yields a prediction for what the corresponding response by the basic sense-only strains co-cultured with the basic secrete-and-sense strain would be. These predictions are shown as curves (one for each [doxycycline]) in fig. S17, and they recapitulate, at least qualitatively, the slow response of the basic sense-only cells. It is important to note that our secretion rates represent mere

'phenomenological secretion rates'. That is, our idealized model does not take into account the aforementioned complex physical scenarios (e.g., collision of cells due to their random jostling motion, cells moving in and out of each others' diffusion field, the precise nature of the cross-over from diffusion-profile to the mean-field (well-mixed) concentration regime). Considering the effect of these scenarios on the secrete-and-sense cells, we conclude that our phenomenological values for *r* are likely overestimates of the actual secretion rate of the basic secrete-and-sense cell. Yet, we found that our values for *r,* which was experimentally adjusted by using the strong promoter *pTET07*, were nonetheless not much higher than the typical secretion rates of the α-factor due to the much weaker endogenous *MFα1* promoter, which the previous models of yeast mating pathway have deduced (*53, 54*). For the highest concentrations of doxycycline that we used, our values for the phenomenological secretion rate *r*, due to the strong promoter *pTET07*, is about 2 times the ~6000 molecules / sec that the previous studies estimated would be produced by the weaker endogenous *MFα1* promoter. However, as insightfully argued by Rappaport and Barkai (*53*), these computed endogenous secretion rates were also likely overestimtaes.

The main point of this section is that Eq. [S6], which describes the pFUS1-GFP response to pure neighbor-communication (i.e., no self-communication) that the basic sense-only cells experience, produces curves whose shapes (slowly rising) and time-scales (slower than response to self-communication) are qualitatively of different from those of the response curves corresponding to pure self-communication (concave down, faster time-scale) described by Eq. [S3]. We showed that these equations recapitulate the main qualitative features of our data (figs. S16 & S17). In the next section, we will consider the integration of self- and neighbor-communication together.

3. Tuning the degree of self-communication and neighbor-communication by varying the receptor expression level and secretion rate

In the previous two sections, we described how a cell would respond to self-sensing and sensing of the other cells, when the two are treated separately. Our goal in this section is to model, through a simple approach, how the secrete-and-sense cell would respond when the two types of sensing occur together. Specifically, we will use Eq. [S3] (describing pure self-communication) and Eq. [S6] (describing pure neighbor-communication) together to compute a phenomenological phase diagram (Fig. 5B) that describes how varying the receptor abundance and the secretion rate can tune the degrees of self- and neighbor-communication for a secrete-and-sense cell.

The main idea behind the secrete-and-sense cell's integration of self- and neighbor-communication (α-factors secreted by self and by the other cells) is that when $G_{others}(t)$ (described by Eq [S6]) is much larger than $G_{self}(t)$ (described by Eq [S3]), then a secrete-and-sense cell predominantly senses the α-factor secreted by the other secrete-and-sense cells. On the other hand, when $G_{self}(t)$ is much larger than $G_{others}(t)$, then a secrete-and-sense cell predominantly senses the α-factor that it secreted rather than sensing the α-factor secreted by the other cells. As we discussed before, the local concentration around the secrete-and-sense cell saturates to a level that is proportional to the cell's secretion rate, whereas the global concentration of the α-factor can increase over time without an upper bound. This allows for a secrete-and-sense cell to self-sense first, then sense the other secrete-and-sense cells. This is responsible for 'timed-

sociability' (Fig. 5C) that we observed in some conditions of Fig. 2C-D. There we found that the basic secrete-and-sense strain responded first and then the sense-only strain responded afterwards. Quantitatively understanding the intermediate scenario, in which both $G_{others}(t)$ and $G_{self}(t)$ are comparable, requires a model for the exchange of the local and global concentrations of the α-factor that occurs between the two components of our liquid culture - the laminar region (below the mixing length scale where the local concentration resides) and turbulent ('well-mixed') region (above the mixing length scale where the global concentration resides). Modeling the interaction and exchange between these two components in this intermediate regime is enormously challenging because there is no known analytical solution to the Navier-Stokes equation that describes this laminar-to-turbulent transition. Numerically modeling this scenario is beyond the scope of our phenomenological toy model and would not yield much intuition. But we do not need to obtain the exact equations to understand the cell's response to the combined self- and neighbor-communication. All our secrete-and-sense strains with constitutive expression of the Ste2 receptor (used in Fig. 2E-F with {0, 0.03, 0.06, 0.09, 0.3, 0.6, 2, 4, 6, 9, 30} μg/ml as dox and heat color range: -250 to 750) have the same secretion system (pADH1-rtTA, pTET-*MFα1*). Thus the secretion rates that we obtained from fitting the data for the basic secrete-and-sense strain (i.e., strain with the endogenous Ste2 promoter expressing *STE2*) in section 2 can be used for the secrete-and-sense strains with constitutive expression levels of Ste2. Note that in our model and Fig. 2E-F, we excluded strong desensitizing cells and dynamics. The only modification that we have to make in modeling the secrete-and-sense (and sense-only) strains with the different constitutive expression levels of Ste2 is to the pFUS1-GFP production function $k([\alpha])$ in Eq. [S2]. $k([\alpha])$ is now different for each of the different strains and depends on their constitutive Ste2 expression levels. This is because as shown in the circuit diagram (Fig. 2B), the receptor level directly affects the pFUS1 promoter that expresses the GFP. In effect, changing the Ste2 expression is equivalent to changing the promoter that expresses the reporter GFP in our strains. More importantly though, the receptor abundance affects the local concentration because Ste2 abundance affects how many α-factor molecules the cell can capture. Intuitively the idea is that for a fixed secretion rate, a low receptor abundance promotes more neighbor-communication due to lack of receptors for capturing self-secreted molecules while a high receptor abundance promotes more self-communication due to the many receptors being able to capture self-secreted molecules. Keeping this in mind, through the procedure mentioned above, we obtain a family of production functions $\{k([\alpha],ste2)\}$, one production function for each constitutive expression level of Ste2. We measured the response of pFus1-GFP for each of the different constitutive expression levels of Ste2 (fig. S9). Then by fitting the following sigmoidal function to the data in fig. S9, for each value of Ste2 expression level (*ste2*):

$$k([\alpha], ste2) = b(ste2) + \frac{V(ste2)[\alpha]^{n(ste2)}}{(K(ste2))^{n(ste2)} + [\alpha]^{n(ste2)}}, \qquad [\boldsymbol{S8}]$$

we obtained the family of production functions $\{k([\alpha],ste2)\}$ (figure S18). In Eq. [S9], b is the basal expression rate. Using the secretion rates motivated by those obtained in section 2 (since all our secrete-and-sense strains have the same secretion system) and values based on $k([\alpha],ste2)$ (fig. S19) in Eqs. [S5-S6], we computed the resulting pFUS1-GFP response $G_{others}(t)$ for each sense-only strain with a constitutive Ste2 expression. Moreover, we computed the resulting $G_{self}(t)$ for each secrete-and-sense strain with a

constitutive expression of Ste2 by using Eq. [S3] and with the local concentration determined by the same procedure as in section 2 but this time, we used the data for the secrete-and-sense strains with constitutive Ste2 expression levels at low OD (Fig. 2E, where self-communication is dominant). The local concentration depends on the Ste2 expression level because the capture efficiency of the α-factor molecules depends on it. Taken together, the procedure described here yields $G_{self}(t)$ and $G_{others}(t)$ for each constitutive expression level of Ste2. To characterize the combination of self- and neighbor-communication, we define the 'degree of sociability' S for each secretion rate and constitutive expression level of Ste2:

$$S \equiv \frac{G_{others}(t \gg \frac{R^2}{D}) - G_{self}(t \gg \frac{R^2}{D})}{G_{others}(t \gg \frac{R^2}{D})} \qquad [\boldsymbol{S9}]$$

Here, $G_{others}(t \gg \frac{R^2}{D})$ is evaluated for the high density (100x) while $G_{self}(t \gg \frac{R^2}{D})$ is evaluated for the very low cell density (1x), for each secretion rate ([doxycycline]) and constitutive expression level of Ste2. $t \gg \frac{R^2}{D}$ indicates that we evaluate G_{self} and G_{others} at any time after the local concentration reaches saturation, which as we saw earlier, occurs on a faster time scale than transcription/translation. So we can choose to evaluate at t at five hours after the co-culture begins. To see the rationale behind defining S in this way, note that after a sufficiently long time G_{others} (evaluated at high cell density) is larger than or equal to G_{self} (evaluated at low cell density). In fact, at the high cell density, G_{others} is essentially equal to the GFP level of both the secrete-and-sense and the sense-only strain due to the large cell density (i.e., 'cell A' and 'cell B' have nearly identical responses as indicated by Fig. 2F). In other words, the secrete-and-sense cell's GFP at the low cell density is not determined by neighbor-communication and is described by G_{self}. At the high cell density, the total GFP level is described by G_{others}. Thus Eq. [S9] states that S=1 is entirely neighbor-communication, S=0 is entirely self-communication. Then computing Eq. [S9] for all the Ste2 expression levels (i.e., using $\{k([\alpha],\text{ste2})\}$) and secretion rates (determined as mentioned in the previous section), we obtain a computed phase diagram shown in Fig. 5B. In this phase diagram we subtracted the basal level fluorescence and imposed a small threshold on S, so that any value of S below the threshold is classified as 'negligible signaling'.

To summarize this section, our computed phase diagram (Fig. 5B), based on Eq. [9], models the main qualitative features of our experiments (Figs. 2E-F). This simple approach models how a secrete-and-sense cell can tune its receptor abundance and its secretion rate to vary its degree of self-communication and neighbor-communication at the same time. This idealized model provides a qualitative insight into the main features observed in our experiments.

4. Interplay between self- and neighbor-communication when positive feedback and active signal degradation (Bar1) are present.

Our main goal in this section is to construct a minimal model to understand how a secrete-and-sense cell uses its positive feedback and an active signal degradation mechanism, such as the Bar1 protease, to respond to self- and neighbor-communication, and produce population-level behaviors.

4. A. Intuitive summary of section 4:

The local α-factor concentration ([α]) that surrounds the secrete-and-sense cell with a positive feedback and a constitutive expression level of the Bar1 protease ([bar1]), is determined by two opposing mechanisms: (1) the positive feedback on the sensed local α-factor that leads to an even higher secretion rate of the α-factor, and (2) the degradation of the α-factor by the Bar1 protease. The local concentration is thus described by

$$\frac{d[\alpha]}{dt} = b + \frac{V[\alpha]^n}{K^n + [\alpha]^n} - \delta[bar1][\alpha] - \gamma[\alpha]\,, \qquad [\boldsymbol{S10}]$$

where b is the rate of basal secretion per cell. The second term here describes the positive feedback on the sensed local α-factor that leads to an even higher secretion rate of the α-factor. It is a sigmoidal-function of [α] because our measurements in fig. S10 show that *pTET07-GFP* level is a sigmoidal function of [α] (note that in our positive feedback strains, *pTET07-MFa1* is responsible for secreting the α-factor, thus *pTET07-GFP* is a direct proxy for the secretion rate of the positive-feedback strains). δ in Eq. [S10] is the degradation constant of the Bar1 protease (the third term in Eq. [S10] describes the first order degradation of the α-factor by Bar1). The last term in Eq. [S10] describes the natural (Bar1-independent) degradation of the α-factor. Without specifying the particular values for any of the parameters in Eq. [S10], it is already clear that solving for $\frac{d[\alpha]}{dt} = 0$ can yield both monostable and bistable steady-state fixed points, depending on the relative magnitudes of the parameters. In fact, the form of Eq. [S10] is similar to many well-studied bistable systems (*65, 66*). But the special feature of this system (and the systems that it mimics such as the cytokine-signaling in T-cells) is that every process described in Eq. [S10] occurs in the extracellular environment, allowing for neighbor-communication to affect the stability conditions. This is what makes our system multicellular, and opens the possibility for intricate collective behaviors of the secrete-and-sense cells. Insightful models of extracellular feedback and degradation that include the multicellular systems-level effects have recently been proposed, particularly in T-cells (*47, 48, 62*). To complement these previous theoretical studies, our experimental system allows us to disentangle and measure the effects of self- and neighbor-communication on the positive feedback and the degradation of the signaling molecule, which has been challenging in previous studies.

The intuitive summary of this section, and of our experimental results, is as follows. Bimodal activation has been observed in our experiments because the threshold for activation, set by the location of the unstable fixed point in Eq. [S10], is highly sensitive to cell-to-cell variation, aided by the high Hill coefficient of the positive feedback. Particularly when the two states (OFF: quiescent state with a very low basal secretion of α-factor, and ON: secreting the α-factor at a maximal rate) are closely separated (due to the high Hill coefficient), this activation-threshold is close to the location of the OFF-state, allowing for cell-to-cell variability to yield a bimodal response at the population level as seen in our experiments. Consistent with the large Hill coefficient of the positive feedback, very short-lived bimodal activation (more transient than when Bar1 is present) is seen in the absence of Bar1 as well. The activiation-threshold is particularly close to the location of the OFF-state when Bar1 is at an

intermediate level (fig. S15). When the Bar1 level is very high, then regardless of the cell density, all secrete-and-sense cells are in the OFF state as they cannot self-activate nor can the cells cooperate to activate each other through their collective basal secretion of the α-factor (the system is monostable - 'OFF') (fig. S14). When the Bar1 level is low but non-zero and the cell density is low, the secrete-and-sense cells rely on self-communication (due to their low basal secretion rate of the α-factor) for their behaviors (since neighbor-communication is negligible). In particular, if the positive-feedback strength is high, then these cells will activate themselves in a bimodal fashion if the activation threshold is close enough to the OFF-state (fig. S15). When Bar1 level is low but non-zero and the cell density is high, self-communication and communication among the secrete-and-sense cells are both important (due to the combined basal secretion rate of the α-factor within the population). In this case, if the Bar1 level is very low, then bimodal activation can disappear because every cell senses the same quorum signal, leading to a monomodal activation at the population level (fig. S15 - Bar1 level = 400 a.u.). But if the Bar1 level is slightly higher and the cell density is high, then the effect of the neighbor-communication is suppressed and the threshold's variability from cell to cell dominates the activation (i.e., more self-activation than neighbor-activation). This can lead to the 'bimodal-activation' seen at the population level (fig. S15 - Bar1 level = 600 a.u.). If the Bar1 level is even higher still and the cell density is high, then self-communication's effect on positive feedback is suppressed by the higher Bar1 level, the threshold for activation is at a higher concentration of the α-factor and the cells rely more on the neighbor-communication for activation. This means that cell-to-cell variability in self-activation is negligible (thus no bimodal activation) and monomodal activation occurs (fig. S15 -Bar1 level = 1600 a.u.). This is also consistent with our observation that self-activation takes a much longer time than neighbor-activation at this Bar1 level (consistent with threshold at a higher α-factor level). In summary, self-activation (due to self-communication) promotes the 'bimodal switching' behavior because of the cell-cell variability in the activation threshold, while neighbor-activation (due to neighbor-communication) promotes monomodal activation as the cells sense the same quorum. Increasing Bar1 level decreases the self-activation and cells rely more on neighbor-communication for activation. These two interactions produce the phase diagrams seen in figs. S14-S15 and Fig. 4D. Below we will try to make these ideas more concrete by calculating each term in Eq. [S10].

4B. Details of calculation: Total degradation rate (3rd and 4th terms of Eq. [S10])

Bar1 is localized in the yeast's periplasmic space where it degrades the local α-factor (our main conclusions, however, do not depend on this localization). This degradation is modeled as a first-order reaction whose rate is $\delta[bar1][\alpha]$, where [bar1] is the constant expression level of Bar1 by the secrete-and-sense cell. More detailed models, such as the insightful models of Rappaport & Barkai (*53*), Jin *et al* (*54*), and Barkai *et al* (*52*) have extensively analyzed this reaction in the context of mating, in which the yeasts need to efficiently find their nearby partners for mating. For our purpose, the important feature is that $\delta[bar1][\alpha]$ increases linearly with $[\alpha]$ for a fixed level of Bar1. As Jin *et al.* (*54*) has argued, a wild-type cell that expresses Bar1 from its endogenous locus is expected to have δ[Bar1] to be roughly 100 times larger than the natural degradation rate of the α−factor ($\gamma=0.01\ s^{-1}$) for the yeast to efficiently find its partner for mating. To relate this

value to a specific expression level of Bar1, we used a flow cytometer to measure the level of GFP that is expressed by the endogenous BAR1 promoter (i.e., pBAR1-GFP) as a function of the exogenous a-factor concentration in a *bar1Δ* strain (fig. S20). Since we also measured the GFP expression level by every one of our constitutive promoters (fig. S8), we could then obtain the relative values of [bar1] for every one of our constitutive promoters by comparison to the pBAR1-GFP level. For the average level of pBAR1-GFP (~2500 a.u., averaged over the dynamic range of pBAR1 shown in fig. S20), we set δ[bar1] ~ 100γ, and as in previous sections, γ=0.01 s^{-1}. This way, we can obtain a range of values for $\delta[bar1][\alpha] - \gamma[\alpha]$. for every one of the secrete-and-sense strains with a constitutively expressed Bar1.

4C. Details of calculation: Total creation rate (1st and 2nd terms of Eq. [S10])

Fig. S10 shows that without the positive feedback, response to α−factor (i.e., the GFP level) for each concentration of doxycycline can be described by a sigmoidal function of [α]. The curves shown in fig. S10 are sigmoidal functions that have been fit to the data shown there, with one sigmoidal curve for each [doxycycline]. When the positive feedback is sufficiently strong ([doxycycline] ≥ 20 μg/ml), according to fig. S10 the secretion rate is a sharp sigmoidal function of [α] while the sigmoid is much less pronounced for smaller values of [doxycycline]. Adding a positive feedback turns this (pFUS1-rtTA, pTET-GFP) circuit into (pFUS1-rtTA, pTET07-*MFa1*) circuit (Fig. 3A, without *BAR1*). That is, the secretion rate, instead of GFP, is now a function of the local concentration [α]. To obtain a 'phenomenological secretion rate' *r* from these GFP levels as a function of the local α−factor concentration, we can use the following two data sets: 1. The estimated range of values for *r* from section 2 (fig. S19: by using Eqs. [S1] and [S3]) for each [doxycycline] (i.e., *r* as a function of [doxycycline]), and 2. The measured pTET07-GFP level as a function of [doxycycline] in fig. S2. Using these two data sets, (i.e., matching the [doxycycline] in the two relationships), we obtained *r* as a function of the GFP level. Then using the relationship between GFP level and [α] (from the fitted sigmoidal curves in fig. S10), we obtained *r* as a sigmoidal function of [α]: *r*([α]). *r*([α]) is due to both the basal and the positive feedback-led secretion. To relate this secretion rate to the rate of change of the local concentration (the first two terms of Eq. [S10]), one would ordinarily need to solve the full three-dimensional diffusion equation with the secretion rate that changes continuously over time *r*([α](t)) and the degradation terms due to Bar1 (with a coupled equation that describes the α−factor expression dynamics). But for our goal of obtaining a simple phenomenological model that intuitively highlights how the two competing mechanisms generate the OFF-ON switch, doing so does not provide much intuition and requires numerically solving the coupled equations. Despite the limitations, for our purpose of obtaining qualitative intuition, we propose to relate *r*([α]) to the creation rate of the local α−factor concentration (sum of the first and second terms of Eq. [S10]) by the following procedure. We first take the derivative of *c(R,t)* (Eq. [S1]) with respect to time to obtain

$$\frac{dc(R,t)}{dt} = \frac{F_0}{2\sqrt{D\pi t}}\left(1 - e^{-R^2/Dt}\right). \qquad [\boldsymbol{S11}]$$

Note that for two local concentrations $c_1(t)$ and $c_2(t)$, with a secretion rate of r_1 and r_2 respectively, we have $(dc_1(R,t)/dt) / (dc_2(R,t)/dt) = r_1 / r_2$ (from Eqs. [S1] and [S7]). Since we have this direct proportionality between *dc/dt* and *r*, and since *r*([α]) is sigmoidal, it

follows that the functional form for the rate of creation of the local α−factor is a sigmoidal function of the form: $b + \frac{V[\alpha]^n}{K^n + [\alpha]^n}$, which is exactly the form of the first two terms of Eq. [S10]. Thus indeed, our analyses in this and previous sections show that the functional forms of all the terms in Eq. [S10] can give rise to binary cell fates. To estimate the first two terms of Eq. [S10], we can pick, for each *r*, *t* to be the time to reach $1 - e^{-1} \approx 0.63$ of the limiting saturation concentration $\frac{RF_0}{D}$ (motivated by the behavior of Eq. [S3]). We computed this *t* for each *r*. This procedure yielded the sum of the first two terms of Eq. [S10].

4D. Details of calculation: Graphically understanding activation properties governed by Eq. [S10]:

By plotting (A) the sum of the first two terms of Eq. [S10] and (B) the sum of the last two terms of Eq. [S10] together, for various values of the positive feedback strength and the Bar1 levels, we can graphically compare the two competing rates to each other. Doing so does not account for all features of our data. But by varying the parameters around these fitted values, we obtained instances where binary and single cell states are possible, with the two situations traversed by varying Bar1 and positive feedback strengths, as in our experiments. This is shown as a graphical argument, showing the competition between creation and destruction rates of local α−factor concentration, plotted for example values, that leads to these cell states (fig. S21). A more detailed model is needed to better account for all the features seen in our experiments and our model is deficient in explaining some of the features. But varying (A) and (B) over the ranges that we found were relevant from the fits to our data, our simple phenomenological model gives a plausible mechanism for how the two competing mechanisms generate OFF and ON states (fig. S21). Neighbor-communication would be equivalent to increasing *b* in Eq. [10]. From fig. S21, we can graphically envision this as the entire 'creation-rate' curve shifting up. Graphically, we can see that depending on the amount of this shift, the entire population can be activated and moved to the 'ON' state. The main idea behind the bimodal activation is that despite the high Hill coefficient associated with the positive feedback, Bar1 provides an activation barrier for the cells to stochastically activate themselves (in the case of self-activation, in low cell density). This can create the bimodal population seen in our experiments. Detailed single-cell modeling, such as the standard Fokker-Planck approximation or Master equation approach may quantify the activation barrier as a function of α-factor, which we will carry out in a future study. To summarize, our minimal, phenomenological model helps us understand the main qualitative features of our measured phase diagrams shown in Fig. 4D.

Discussion

In summary, we have shown that our simple mathematical model, despite using idealizations, can provide insights into the main features that we observed in our experiments. One could extend both our experimental work and mathematical model to a larger set of scenarios that we did not have the space to investigate here. Our work focused on the fundamental secrete-and-sense circuit motif that is seen in nature. But one could combine our analyses of the different circuit configurations to draw conclusions about some of the more complex regulation schemes that can be built by combining these

simpler motifs that we analyzed. A future work that looks at the effect of various spatial multicellular structures (*72*, *78, 82, 83*) would yield further insights into the design principles that underlie the secrete-and-sense circuits. Many systems that use the secrete-and-sense circuits, such as the T-cells and bacteria that sense their quorum, often work in settings where there is no spatial structure, which our work most directly applies to. But since diffusion gradients are formed in both our liquid cultures and in spatial structure settings, our findings are applicable and can be extended to spatial structures as well (e.g., local concentration responsible for self-communication in both cases). Indeed, our work recapitulated many behaviors that have been observed in naturally occurring secrete-and-sense cells that have spatial structures. Our work focused on the most fundamental aspects of the secrete-and-sense circuits and revealed their design principles in the simplest yet widely applicable settings. By doing so, we showed how a single class of circuits can be continuously tuned to realize a wide range of social behaviors, including those observed in very different biological systems (e.g., T-cells, quorum sensing bacteria), under one unified framework. The approach that we have used in our model and experiments may aid on-going efforts to reveal the design principles of other fundamental motifs of multicellular 'cell-circuits' (*62*) in nature.

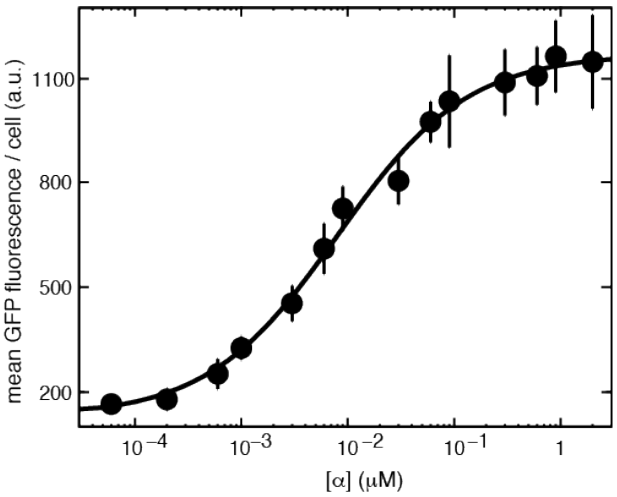

Fig. S1.

Reporter GFP expressed by the promoter *pFUS1*, which is induced at various levels by varying the concentration of the α-factor. Here we used the strain ('CB009' in table S1) that serves as the parent of all our secrete-and-sense and sense-only strains. Various amounts of the α-factor were exogenously added to the liquid culture containing CB009. After three hours of incubation in each level of the α-factor, we used a flow cytometer to measure the mean single-cell GFP fluorescence. A previous study (*14*) on this strain showed that pFUS1 reaches maximal activity for each a-factor concentration after 90 minutes in induction. Black curve represents a sigmoidal transfer function $k([a])$ in Eq. [S2], that fits the data. Error bars, s.e.m. n=3.

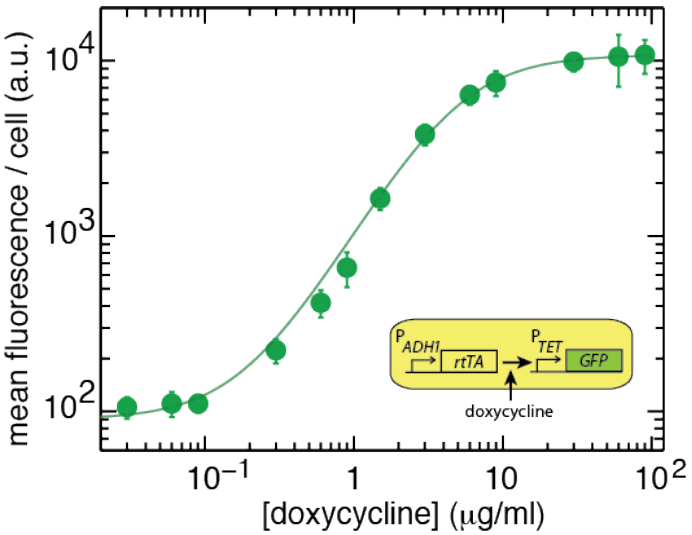

Fig. S2.

Expression level of GFP due to *pTET07* as a function of the doxycycline concentration. We used the strain ('Hy8y' in table S1) that expressed pTET07-GFP (with pADH1-rtTA) and a flow cytometer to measure the steady-state mean single-cell GFP level at various concentrations of doxycycline. All our secrete-and-sense strains use the same *pTET07* to secrete their α-factor. Hence this plot shows the inducibility of *pTET07* in all our secrete-and-sense strains with *pADH1* expressing *rtTA* (i.e., secrete-and-sense strains used in Fig. 2). Green curve represents a sigmoidal transfer function obtained by fitting to the data. Error bars, s.e.m. *n*=3.

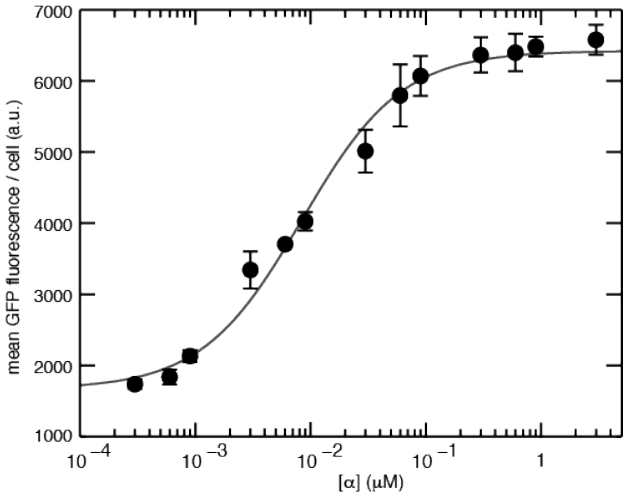

Fig. S3.

Characterization of the endogenous *pSTE2* promoter used in our 'basic secrete-and-sense' and 'basic sense-only' strains (used in Fig. 2, C and D). Here we used the strain ('Hy221y' in table S1) with *pSTE2-GFP*. After 2 hours of incubation in each concentration of the exogenous α-factor, we used a flow cytometer to measure the mean single-cell GFP fluorescence. Black curve represents a sigmoidal transfer function obtained by fitting to the data. Error bars, s.e.m. n=3.

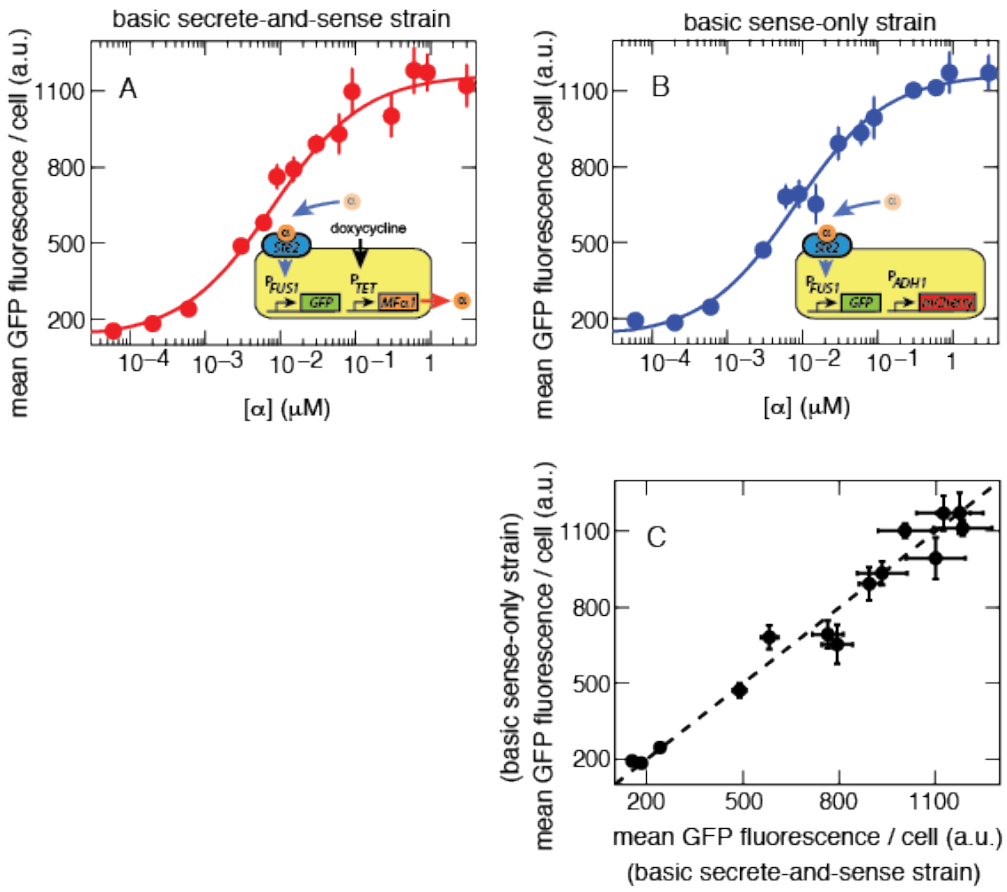

Fig. S4

Response of the basic secrete-and-sense and the basic sense-only strains to various concentrations of exogenously introduced α-factor are identical. In both 'basic' strains, Ste2 is expressed by its endogenous pSTE2 promoter. **(A)** The basic secrete-and-sense strain's mean single-cell GFP level to exogenously introduced α-factor after three hours (at [doxycycline]=0 μg/ml, no secretion). Red curve is the sigmoidal function that fits the data. **(B)** The basic sense-only strain's mean single-cell GFP level to exogenously introduced α-factor after three hours. Blue curve is the sigmoidal function that fits the data. **(C)** The basic secrete-and-sense and the basic sense-only strains' GFP levels (A and B respectively) plotted against each other for comparison shows that the two strains have an identical response to the exogenous α-factor. Error bars, s.e.m. *n*=3.

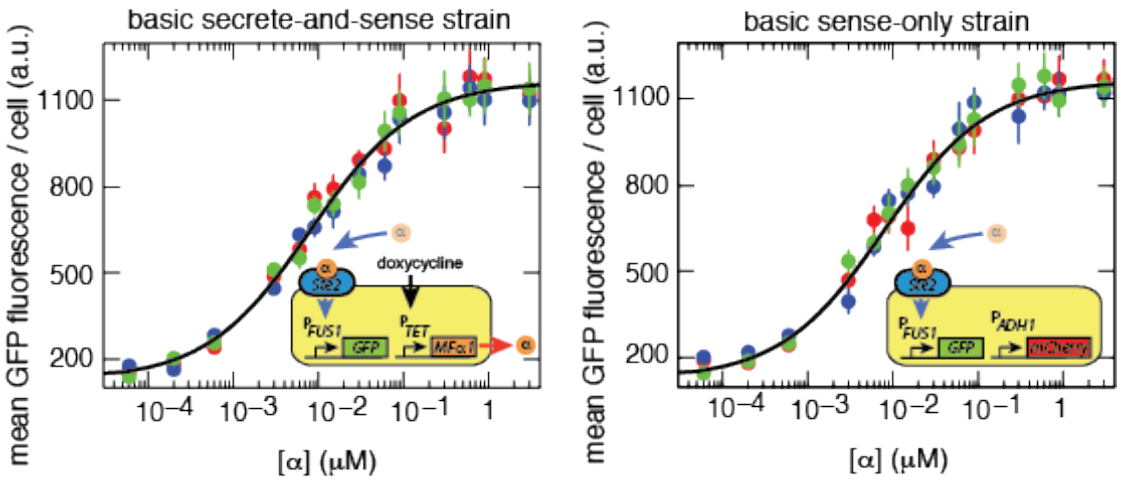

Fig. S5

Response of the basic secrete-and-sense strain and the basic sense-only strain to the exogenously introduced α-factor are not titrated by the range of the ODs we used in our experiments. That is, we do not observe significant dilution of the α-factor in the media by a higher OD of cells than in a lower OD of cells in the time scale of our experiments. In both 'basic' strains, Ste2 is expressed by its endogenous pSTE2 promoter. **(A-B)** By growing the secrete-and-sense strain (A) and the basic sense-only strain (B) at OD=0.1 (red), 0.01 (blue), and 0.001 (green) in the presence of exogenously introuced α-factors for three hours, we did not observe any significant variation in the GFP levels at the three different ODs for either strains due to potential titration of α-factors by the differing densities of cells. Hence in our co-culture experiments in the main text, there is no significant titration of the α-factor secreted by the secrete-and-sense strains due to a high density of sense-only cells. In other words, co-culturing a secrete-and-sense strain with a sense-only strain, both at the same OD, does not yield a result that would be different from that of a co-culture with different ODs between the two strains (as long as the same OD is used for the secrete-and-sense strain for both co-cultures) due to any α-factor titration effects. Black curves are fits to OD=0.1 for secrete-sense strain (A) and for sense-strain (B). Error bars, s.e.m. *n*=3.

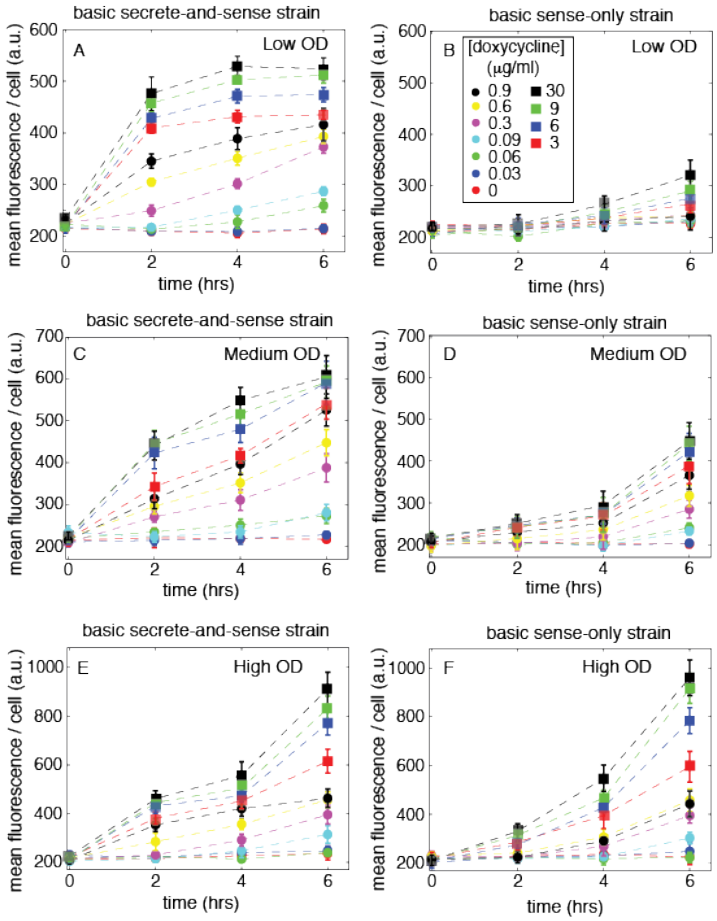

Fig. S6

Time-courses representing the co-culture of the basic secrete-and-sense strain with the basic sense-only strain at various cell densities (OD) and secretion rates ([doxycycline]). In both strains, Ste2 is expressed by its endogenous promoter pSTE2. Subset of these data are shown in Fig. 2, C and D. Flow cytometer measurements of the mean single-cell fluorescence of the basic secrete-and-sense and the basic sense-only strains with equal ratio seeding for approximate initial total ODs of (A-B) 0.001, (C-D) 0.005, and (E-F) 0.1. During the six hours of co-culture, there was less than a 10-fold increase in the overal OD of the co-culture. Both strains were normalized to equal volumes by using the scatter distributions observed in the in the flow cytometer. Cells can be hyperactivated or desensitizd which are important for long time scales. We limited our cultures to shorter times and excluded such cells, and normalized cell size changes. Much longer culturing times lead to secrete-and-sense cells desensitizing first before sense-only. Note that the three co-cultures (A-B, C-D, E-F) all maintain the same fold-difference among themselves during the time-course (e.g., low OD and high OD are different by ~100-fold during the time course). Error bars, s.e.m. n=3.

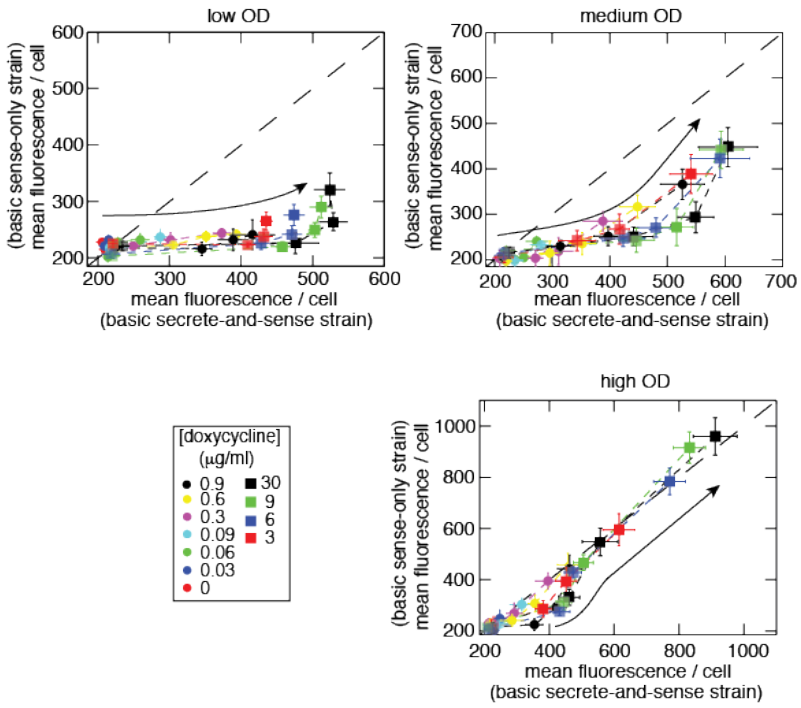

Fig. S7

Trajectories, over time, followed by the basic secrete-and-sense and the basic sense-only strains in their co-culture. In both strains, Ste2 is expressed by its endogenous promoter. The data shown here are the same data as in fig. S6, but now plotted as trajectories in the 'GFP expression-plane', for ease of comparision between the response of the basic secrete-and-sense and that of the basic sense-only strain. Arrows indicate the general trajectory that the co-culture follows over time (i.e., time increases in the arrow's direction). Error bars, s.e.m. *n*=3.

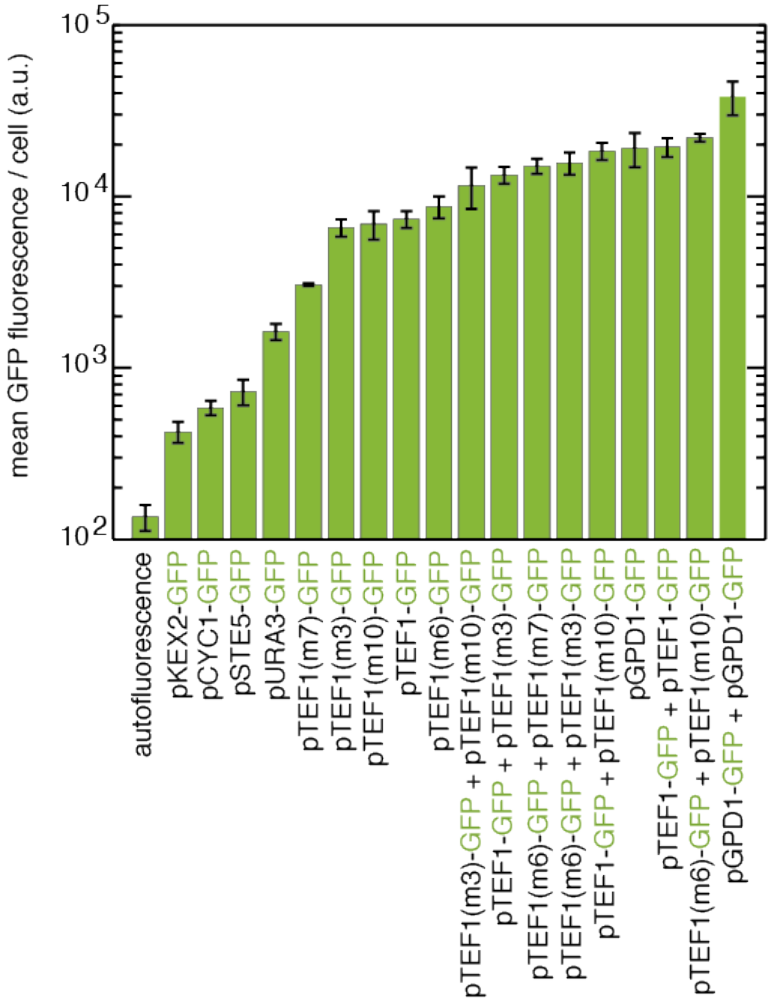

Fig. S8

Strength of the constitutive promoters used in our study measured by GFP expression. For each constitutive promoter, we constructed a strain that expressed GFP through that promoter. Plotted here are the resulting mean single-cell GFP levels in these strains. Subsets of these promoters were used in this study to constitutively express *STE2* and *BAR1* (see Table S1 for specific strains). pTEF1(m#) refers to TEF1 promoter variants (*101, 102*). Error bars, s.e.m. *n*=3.

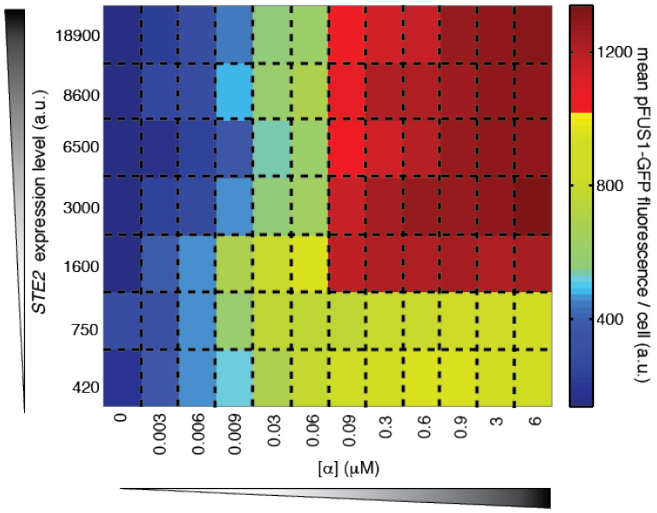

Fig. S9

pFUS1-GFP level in the sense-only strains that constitutively express STE2. The seven sense-only strains, each with a different constitutive expression level of Ste2 (indicated by the 7 rows in this heat map, one row for each strain, strength of constitutive promoter determined in fig. S8 and rounded), were grown in a media with an exogenously introduced a-factor. This heat map shows how changing the Ste2 expression level affects the level of the reporter GFP expressed by pFUS1 (the effect of changing Ste2 on pFUS1-GFP in secrete-and-sense strains is identical to this). Each pixel is the mean single-cell GFP fluorescence after 3 hours of culturing in exogenous α-factor and is an average of 3 independent experiments. These measurements were obtained with a flow cytometer. Note that at [α]=0 μM (first column), every strain has the same basal level of fluorescence, no matter how much Ste2 is expressed. Thus there is no false activation of pFUS1-GFP due to an increased level of Ste2.

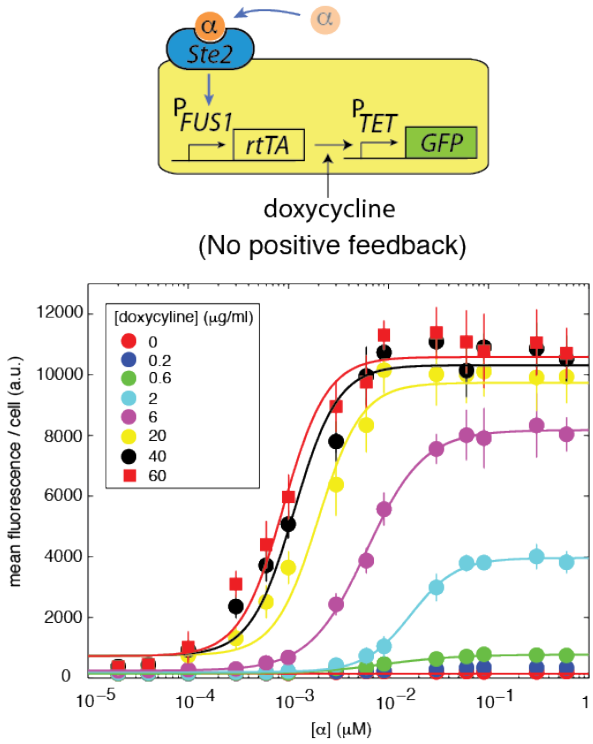

Fig. S10

The transfer functions measured here, using the strain shown above, characterizes the "positive-feedback strength" as a function of the doxycycline concentration for all the secrete-and-sense strains with the positive feedback link used in Figs. 3 and 4 (including those with Bar1 expression). Both the strain shown above and the secrete-and-sense strains with the positive feedback link, have the same (*pFUS1-rtTA, pTET07-GFP*) circuit as a reporter. And the secrete-and-sense strains in Fig. 3 also have *pTET07-MFa1* that is used for secretion of the a-factor. Hence the *pTET07-GFP* is is a proxy of the secretion rate as well as the positive feedback strength. For a fixed concentration of doxycycline for seven hours, we grew above strain alone in the presence of exogenously introduced α-factor for two hours. The resulting data was fit by a sigmoidal funciton. Doing so for various doxycycline concentrations, we obtained a family of sigmoidal fit curves above. As shown, increasing the doxycycline increases the sharpness of the cell's response to the α-factor. These curves define and quantify the 'strength of positive feedback' in the secrete-and-sense cells used in Fig. 3. Error bars, s.e.m. n=3.

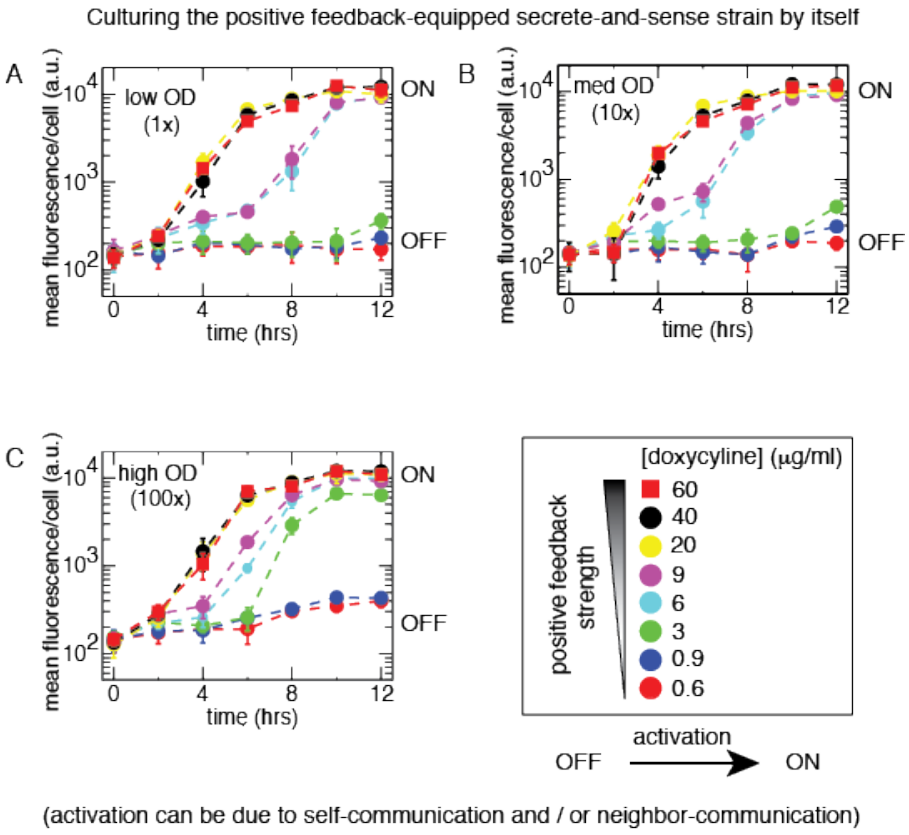

Fig. S11

Time-courses showing the mean single-cell GFP level of the secrete-and-sense strain with the positive-feedback (strain shown in Fig. 3A) when it is grown by itself. Each panel shows, for a given cell density, the activation dynamics in cultures with different doxycycline concentration (positive feedback strength). Low cell density (OD=0.001 (1x)), medium cell density (OD=0.01 (10x)), and high cell density (OD=0.1 (100x)). These plots, along with those in fig. S12, quantify the representative histograms of single-cell fluorescence shown in Fig. 3, B and C. Here, we can see that increasing the positive feedback strength (i.e., increasing the doxycycline concentration) increases the speed with which activation occurs. Note that since the strain's growth rate does not depend on the initial OD, 1x, 10x, and 100x represent the relative ODs between the three different cell density cultures at all times. Error bars, s.e.m. n=3.

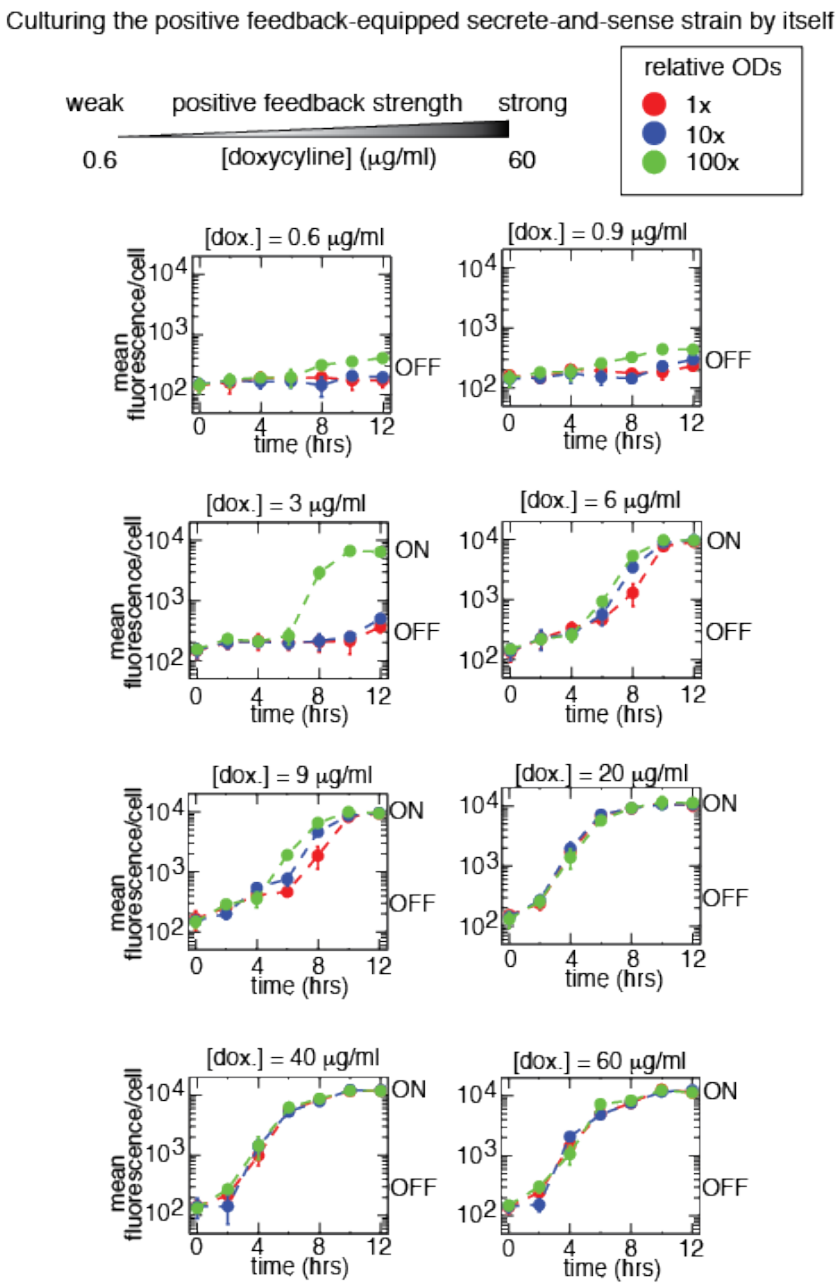

Fig. S12

Time-courses showing the mean single-cell GFP level of the secrete-and-sense strain with the positive-feedback (strain shown in Fig. 3A) when it is grown by itself. Here, same data as those used in fig. S11 is plotted but now each panel shows the activation dynamics in cultures at three different cell densities and for a fixed [doxycycline]: Low cell density =0.001 (1x), medium cell density = 0.01 (10x), and high cell density =0.1 (100x). These plots quantify the representative histograms of single-cell fluorescence shown in Fig. 3, B and C. Herer we see the role of cell density for a fixed doxycyline concentration. Importantly, note that for [doxycycline]=3μg/ml (weak positive feedback strength), cells in the low (1x, red curve) and medium (10x, blue curve) cell density cultures remain inactive (in the OFF-state: basal flurescence level ~ 150 a.u.) but they are activated in the high cell density culture (100x, green curve). This indicates that at the high

cell density, neigbor-communication is responsble for the activation (due to many cells collectively amplifying each cell's small basal secretion of the a-factor) -- an example of 'neighbor-activation'. When positive positive feedback strength is slightly higher but not too strong ([doxycycline]=6 μg/ml, 9 μg/ml), self-activation takes place at the low cell density (1x) and neighbror-communication speeds up self-activation at the higher cell densities (i.e., graphically this is seen by the fact that the blue curve lies above the red curve, and the green curve lies above the blue curve). Error bars, s.e.m. *n*=3.

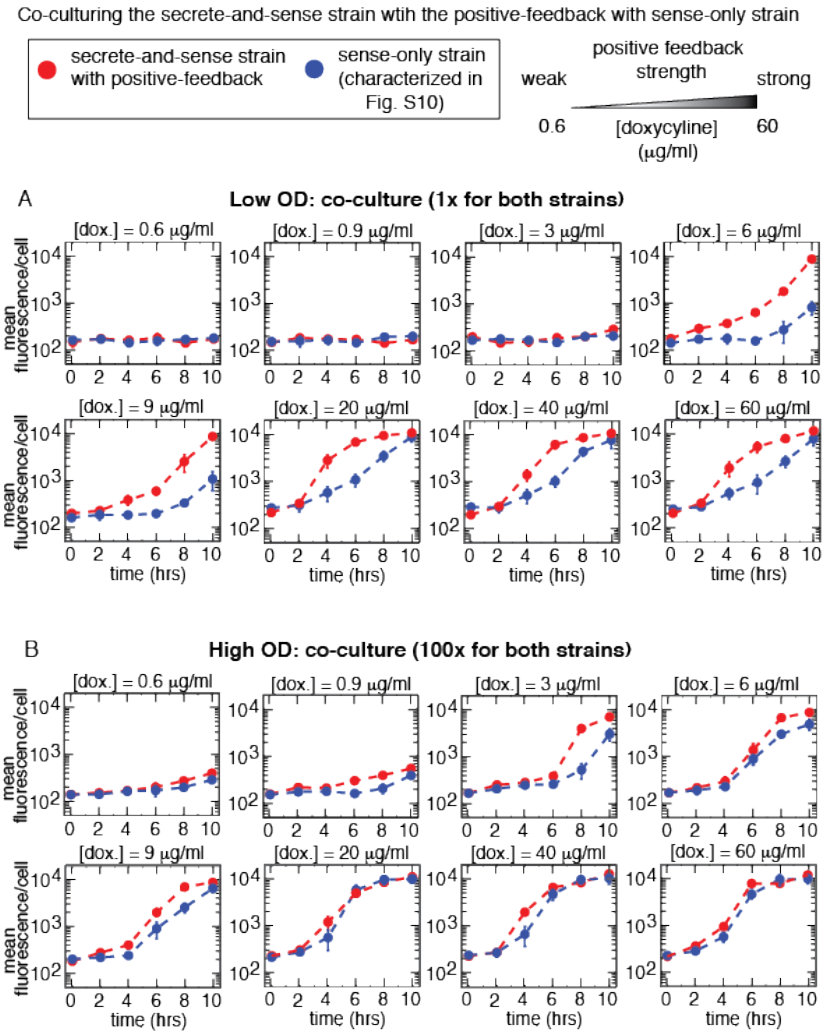

Fig. S13

Co-culturing the secrete-and-sense strain with the positive feedback link (strain in in Fig. 3, A-C) with its partner sense-only strain (characterized in fig. S10) shows that in co-cultures with a low cell density (1x: approx. OD=0.001 for the co-culture), the degree of neighbor-communication is low for activation of the secrete-and-sense strain while at the high cell density (100x: approx. OD=0.1 for the co-culture), neighbor-communication is primarily responsible for activation of the secrete-and-sense strain. Note in low cell density cultures (1x), sense-only strain (blue curve) has lower GFP levels than secrete-and-sense cells until the later is fully activated (and maximally secreting α-factor). Each strain first incubated in dox before combined. The main point here is: At low density, secrete-and-sense strain's GFP had higher than sense-only over time until sense-only caught up, while at the high density both had nearly identical GFP traces. Thus each positive feedback enabled secrete-and-sense cell self-activates at the low cell density without the aid of its neighboring cells. At the high cell density (100x), the sense-only cells' GFP level increases over time, even before the secrete-and-sense cells are fully activated. This indicates neighbor-activation. Note also that in fig. S12, we saw that for [doxycycline] = 6 μg/ml, the secrete-and-sense cell could not self activate in the low cell density culture but activated at high cell

density culture. This again supports the conclusion that neighbor-activation takes place in this high cell density. Error bars, s.e.m. *n*=3.

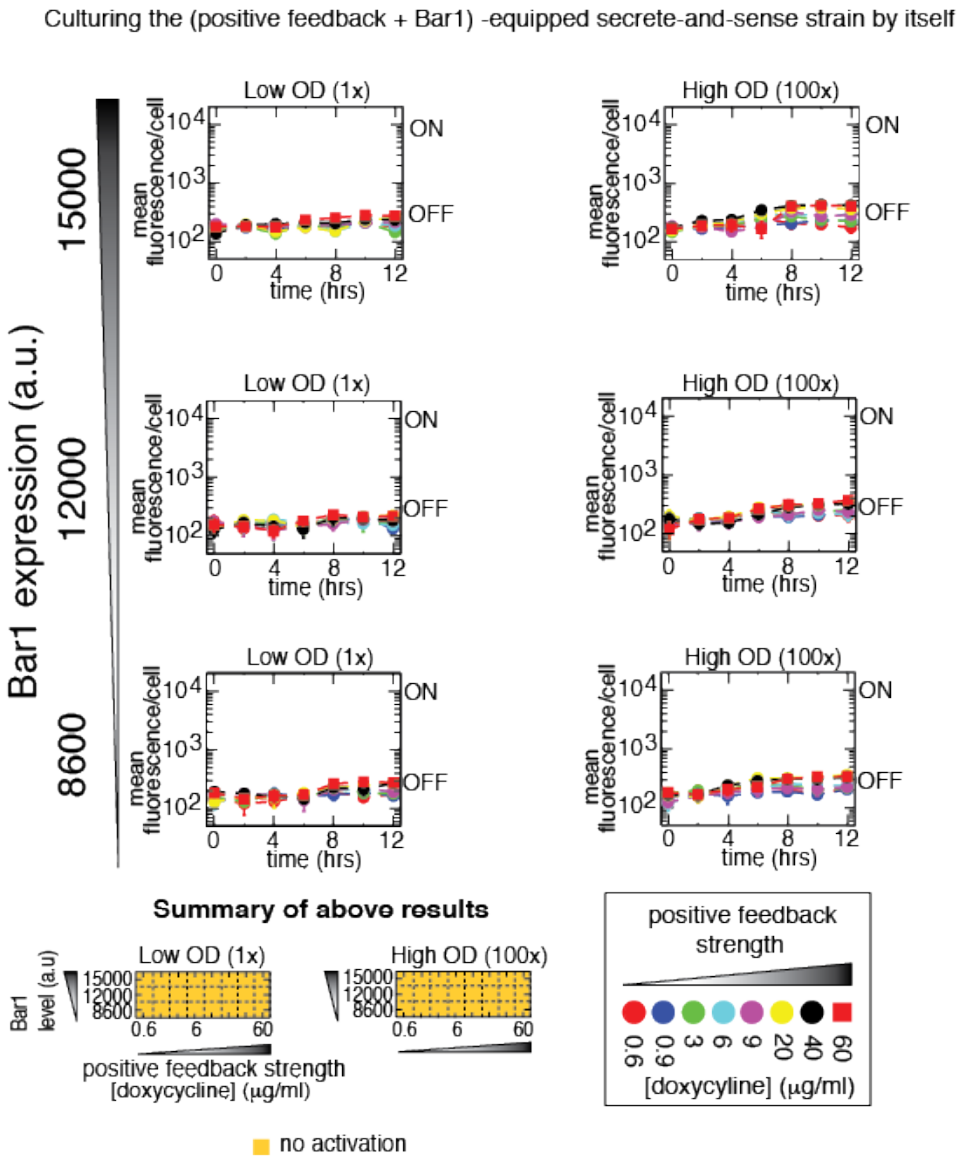

Fig. S14

Full set of time courses that shows the activation dynamics of three of the secrete-and-sense strains that have a positive-feedback and a constitutive expression of Bar1 (strains shown in Fig. 3D, see table S1 for the list of strains). Each strain was cultured by itself in various concentrations of doxycycline and in low (OD=0.001) and high (OD=0.1) cell densities. The Bar1 expression level was determned by measuring the strength of the constitutive promoters (fig. S9). Here we show three strains, each with a high Bar1 expression level (top three rows of the measured phased diagram in Fig. 4D). By analyzing each of these time courses, we constructed partial phase diagrams (comprising the top three rows of the phase diagrams shown in Fig. 4D) at the bottom of this figure. Each pixel summarizes a single time-course. 'No activation' means that within the bounds of OD that we investigated, cells do not turn on during the time-course. Conclusion from this figure is that at these high levels of Bar1, no matter how strong the positive feedback is, the secrete-and-sense strain remains inactive. Error bars, s.e.m. *n*=3.

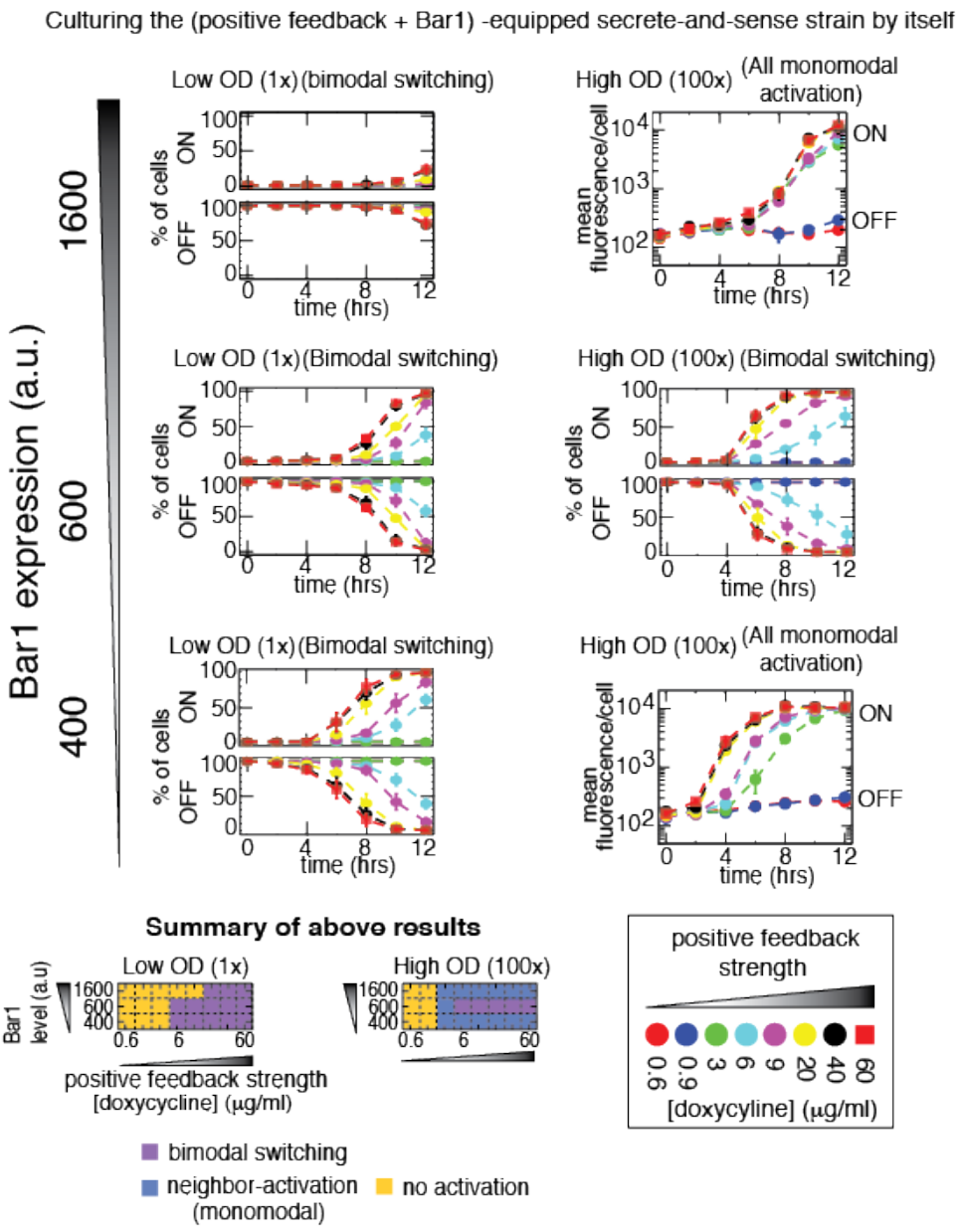

Fig. S15

Full set of time courses that shows the activation dynamics of three of the secrete-and-sense strains that have a positive-feedback and a constitutive expression of Bar1 (strains shown in Fig. 4A, see table S1 for the list of strains). Each strain was cultured by itself in various concentrations of doxycycline and in low (OD=0.001) and high (OD=0.1) cell densities. The Bar1 expression level was determned by measuring the strength of the constitutive promoters (fig. S9). Here we show three strains, each with a medium to low Bar1 expression level. In scenarios where mono-modal activation (graded, uniform activation) is observed, the mean single-cell GFP fluorescence is plotted. In scenarios where we observe biomodal populations (each cell digitally responds as 'OFF' or 'ON', as shown by the histograms in Fig. 4B and 4C), which we call 'bimodal switching' here, we gated the two subpopulations of cells (within the mono-clonal culture) and recorded the percentage of the population that is ON or OFF. We used the same gating for a given

doxycycline concentration acorss the different strains to ensure a fair comparison. By analyzing each of these time courses, we constructed partial phase diagrams (comprising the second, third, and the fourth rows from the bottom in the phase diagrams shown in Fig. 4D) at the bottom of this figure. Each pixel summarizes a single time-course. 'No activation' means that within the bounds of OD that we investigated, cells do not turn on during the time-course. 3 μg/ml doxycycline condition for bar1 expression = 350 is monomodally activated by the high cell density and is shown in Fig. 4D (weak feedback strength). It is important to note that for Bar1 = 600 a.u., in the high cell density culture, bimodal switching is observed but it also represents neighbor-actiation. Indeed comparing the OFF vs ON trajectories in the low and high cell densities, we see that the 100-fold increase in cell density increaess the rate of activation. In the model section 4A, we provide an intuitive reasoning behind the phase diagram shown here. Error bars, s.e.m. n=3.

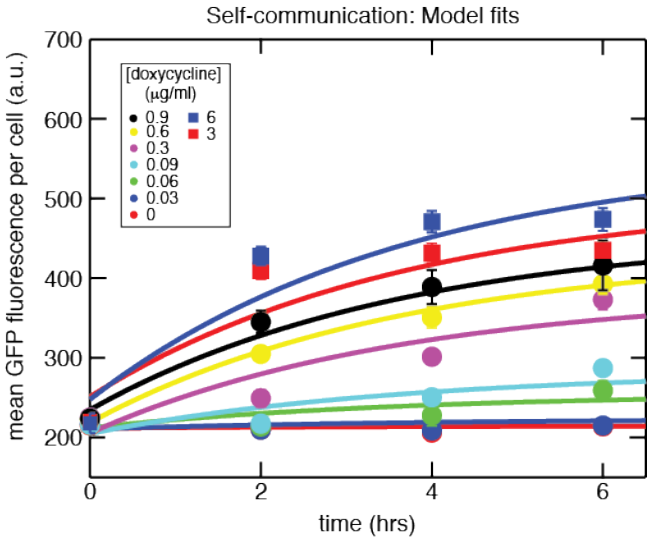

Fig. S16

Fitting our model for the basic secrete-and-sense strain's pFUS1-GFP level due to pure self-communication (Eq. [S3]) to our data. Curves represent the best fits of Eq. [S3] to the data points. Here we used the data for the basic secrete-and-sense strain (i.e., the secrete-and-sense strain with the endogenous Ste2 promoter expressing Ste2). For other expression levels of Ste2, our model is summarized in the computed phase diagram shown in Fig. 5B (for these secrete-and-sense strains, our model produces similar temporal dynamics as seen here for the endogenous expression of Ste2). Here we used data for the lowest OD (1x) (also shown in Fig. 2C and fig. S6) in which pure self-communication (negligible neighbor-communication) takes place. More detailed model would better fit this data and our model is limited. The important feature here is that Eq. [S3] produces the response to self-communication (curves in this figure) which has a qualitatively different shape than the response to neighbor-communicaiton that is described by Eq. [S6] (curves shown in fig. S17). Note that for high doxycycline concentrations (i.e., high secretion rates), there is noticeable neighbor-communication among the secrete-and-sense cells as well as self-communication. The curves here, described by Eq. [S3], only represent self-communication. For details of the physical considerations that have been left out of our idealized model, see the section on model description. Error bars, s.e.m. n=3.

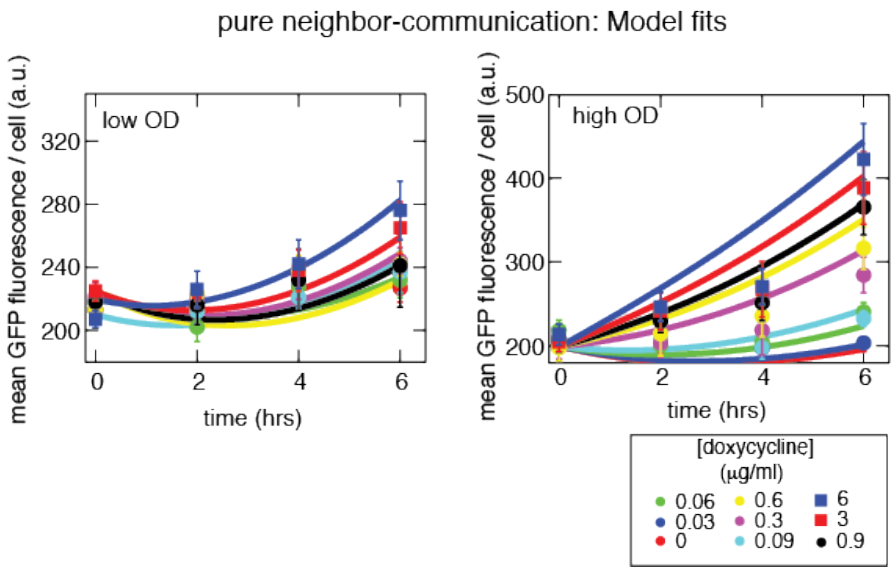

Fig. S17

Fitting our model for the basic sense-only strain's pFUS1-GFP response to neighbor-communication (Eq. [S6]) to our data. Here we use the sense-only strain with the endogenous expression of Ste2 (using the native STE2 promoter). For the other expression levels of Ste2, our model fits are summarized in the computed phase diagram in Fig. 5B (for these secrete-and-sense strains, our model produces similar temporal dynamics as seen here for the endogenous expression of Ste2). These data points are the same as the ones shown in fig. S6. Low total cell density 1x and high total cell density 10x. More detailed model would better fit this data and our model is clearly limited. For the co-cultures with a very high cell density, our model's mean-field approximation for global concentration is invalid (details in sections 2 and 3 of our model description) and does not fit the data. As in fig. S16, the important feature here is that Eq. [S3] produces the response to self-communication which has a qualitatively different shape and time-scale than the response to neighbor-communicaiton that is described by the curves shown here (Eq. [S7]). Error bars, s.e.m. n=3.

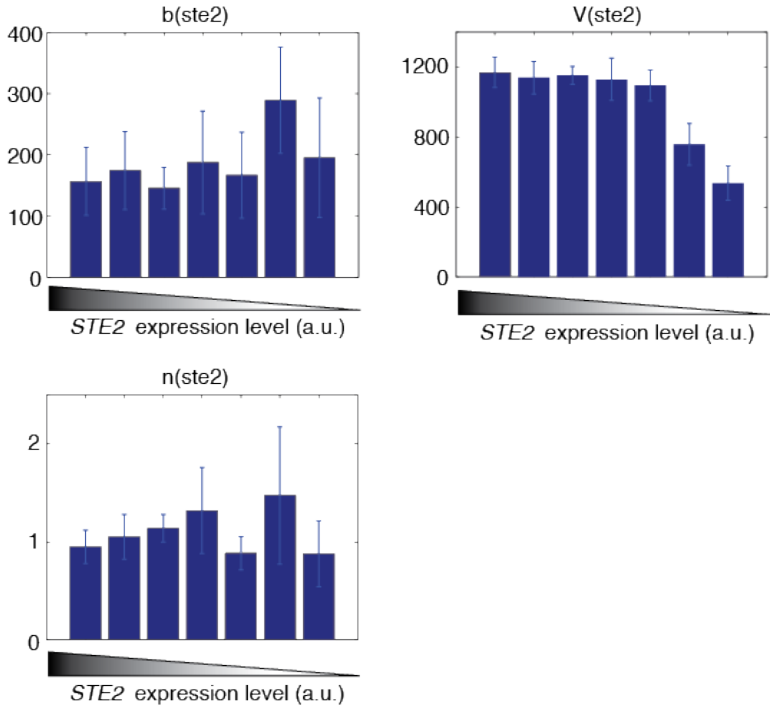

Fig. S18

Fitting parameters of Eq. [S8] to data in fig. S9 (strains listed in fig. S9 and in the heat maps of Fig2). These parameters are used to compute the phase diagram shown in Fig. 5B (see Eq. [S9]). In other words, these parameters aid in determining the secrete-and-sense cell's response when both self- and neighbor-communication affects it. Error bars are 95%-confidence intervals of the fits.

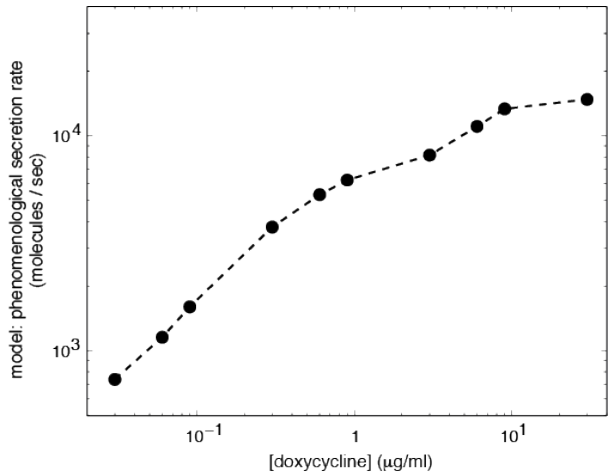

Fig. S19

Phenomenological secretion rates as a function of doxycycline concentration used in our model for computing the phase diagram in Fig. 4B. These numbers were derived based on our model for the basic secrete-and-sense strain (i.e., with endogenous STE2 promoter expressing Ste2) as a function of the concentration of doxycycline (see model sections 1 & 2). Specifically, these rates were derived from the local-concentration around the cell by assuming steady-state net flux, which is a combination of consumption and actual secretion rate. The secretion system is the same for the secrete-and-sense strains with various constitutive expression levels of Ste2. As mentioned in the model sections 1 & 2, our model combines several effects, and lumps them into this one 'phenomenological' secretion rate. Thus the actual secretion rate is likely lower than the phenomenological secretion rates reported here. More detailed explanations of this rate are given in the model description sections. Our idealized model uses these values for the secretion rate to produce the phase diagram (Fig 5B) and response curves (fig.S 17) to model the main features of our data.

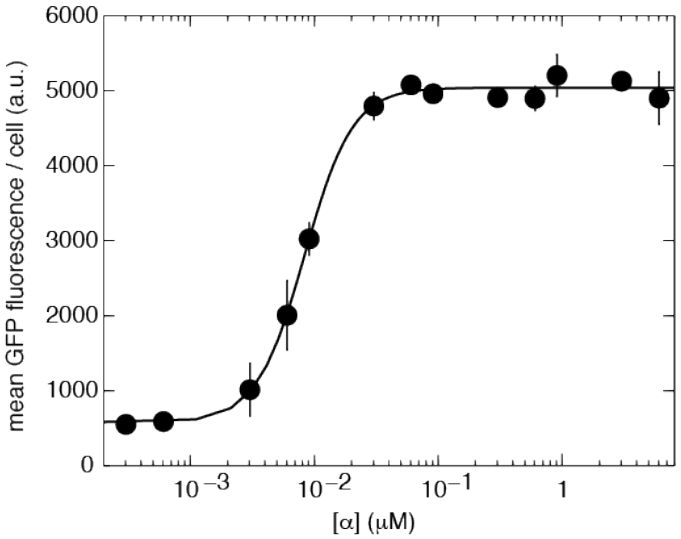

Fig. S20

pBAR1-GFP level measured in a *bar1Δ* background strain for various concentrations of exogenously introduced α–factor. Cells were incubated for two hours in the exogenously introduced α-factor before their mean single-cell pBAR1-GFP fluorescence was measured by a flow cytometer. This plot was used in our model (Section 4) to compute the relative expression levels of Bar1 in the secrete-and-sense strains that constitutively expressed Bar1 (used in Fig. 4). Specifically, in our model, these measurements allowed us to set the relative value for the degradation rate $\delta[bar1][\alpha]$ in Eq. [S10] for all our secrete-and-sense strains that expressed Bar1 (see model section 4 for more detailed explanations). Error bars, s.e.m. n=3.

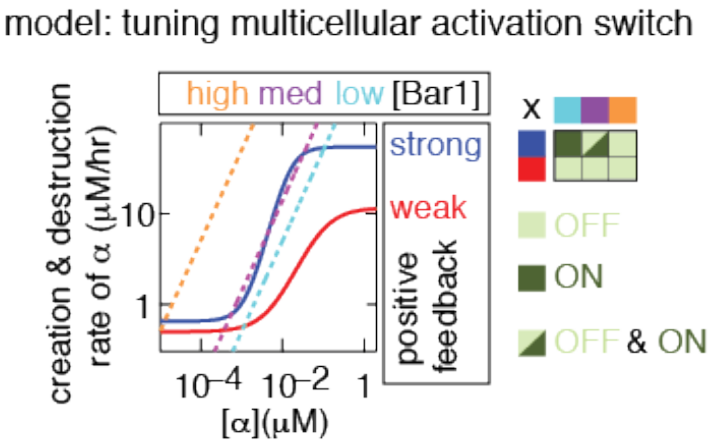

Fig. S21

From our model, we can compute the competing rates (creation and destruction rates of the local α-factor concentration, Eq. [S10]) that can lead to OFF-state and ON-state for the secrete-and-sense strains with the positive feedback and constitutive expression of Bar1. Here, we graphically show a plausible mechanism for how the two competing rates can generate these two states (see our model description in section 4 for details). The range of example destruction rates chosen for this plot for the high, medium, and low Bar1 levels are motivated by our measurements of the Bar1 expression levels (fig. S20) and the range of strengths of the constitutive promoters (fig. S8). The creation rate curves due to the strong and weak positive feedback were motivated by the values obtained from our fits (based on fig. S10 and procedure described in section 4 of our model description) and are meant to be taken as example values. More detailed model will likely better account for all the features seen in our experiments. Using the graphical reasoning of the type presented here, one can understand the main qualitative features of our measured phase diagrams shown in Fig. 4D.

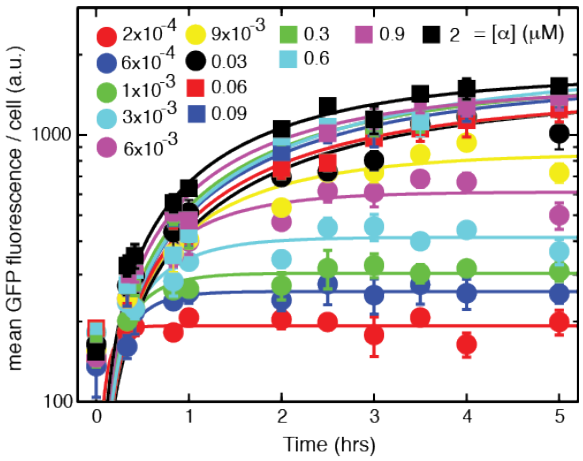

Fig. S22

Dose response to α–factor over time for pFUS1-GFP (sensor for α–factor used in our study) using the strain CB9r (table S1). These data support the quasi-steady state approximation that we used to model the time course of our experiments for the short time scales. Curves represent best fits to the standard first order expression and degradation equation. Error bars, s.e.m. *n*=3.

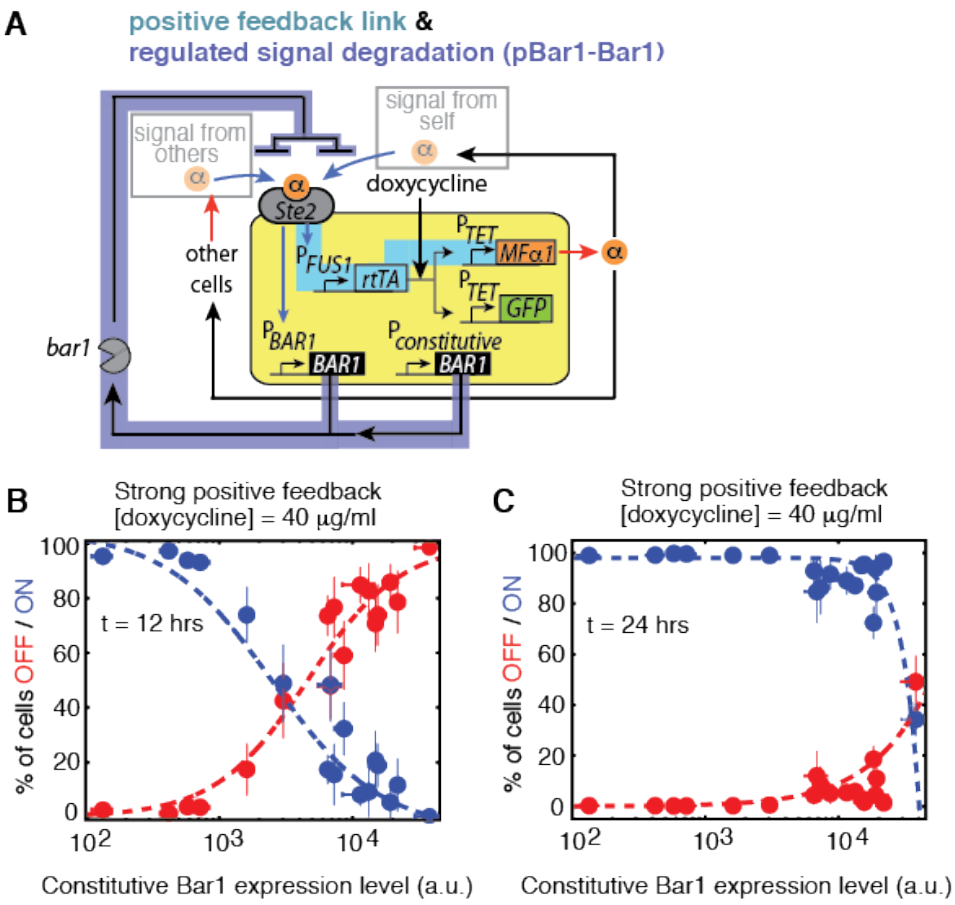

Fig. S23

Secrete-and-sense strains with the positive feedback link and an "adaptive" signal-degradation mechanism (pBAR1-Bar1; 17 strains in table S1) transition from the OFF-state (quiescent state) to the ON-state (maximally secreting state) more slowly than the cells with constitutive expression of Bar1 alone (i.e., strains shown in Fig. 4A). **(A)** Circuit diagram of a secrete-and-sense cell with postiive feedback and two copies of BAR1. One copy of BAR1 is expressed by a constitutive promoter. The other copy is expressed by the endogenous promoter pBAR1 that is upregulated by the α–factor (see pBAR1-GFP characterized in fig. S20). Thus this cell increases its Bar1 expression level as it senses more α–factor. By swapping the constitutive promoter, we generated a library of strains of this type (constitutive promoters are characterized in fig. S8). Each strain in this library has been cultured by itself with the starting OD of 5×10^{-4} for **(B)** 12 hrs and **(C)** 24 hrs with [doxycycline] = 40 μg/ml (i.e., strong positive feedback). Using flow cytometry, we determined the percentages of the OFF (red) and ON (blue) subpopulations for each strain as a function of the constitutively expressed portion of the total Bar1 level (different data points represent different strains). These strains maintain a bimodal population of functionally distinct cells (OFF: quiescent, ON: fully secreting) for a longer time than their counterparts in Fig. 4. Even with the strong positive feedback ([doxycycline] = 40 μg/ml), several of these strains switch from OFF to ON sufficiently slowly that they maintain noticeable levels of the two distinct subpopulations after 24 hours (C). Error bars, s.e.m. *n*=3.

Table S1.

List of yeast strains used in this study

HygB denotes a hygromycin B resistance gene. *KanMX* denotes G418 (Geneticin) resistance gene.

Strain	Immediate parent strain	Genotype	Description & figure it is used in
BY4741	- - -	*MATa BAR1 FAR1 his3 leu2 met15 ura3*	Background strain (Source: Open Biosystems)
BY4741r5	BY4741	*MATa HygB BAR1 FAR1 his3 leu2 met15 ura3 pADH1-rtTA*	Background strain: Allows doxycycline-induction
CB008	W303	W303 *MATa far1Δ his3 trp1 leu2 ura3*	Background strain (Source: Supplementary Ref. 14)
CB8HYDB	CB008	*KanMX MATa far1Δ bar1Δ his3 trp1 leu2 ura3*	Background strain
CB008r2	CB008	*far1Δ his3 trp1 leu2 ura3 pADH1-rtTA*	Background strain Allows doxycycline-induction
CB8F1	CB008	*HygB far1Δ his3 trp1 leu2 ura3 pFUS1-rtTA*	Background strain: Requires a-factor for doxycycline-induction
CB8F1DB	CB8F1	*KanMX HygB far1Δ bar1Δ his3 trp1 leu2 ura3 pFUS1-rtTA*	Background strain: Requires a-factor for doxycycline-induction: (*far1Δ bar1Δ*)
CB009	CB008	*MATa far1Δ bar1Δ his3 trp1 leu2 ura3 mfa2::pFUS1-GFP*	fig. S1: background strain for all secrete-and-sense & sense-only strains (Source: Supplementary Ref. 14)
CB009r5	CB009	*HygB far1Δ bar1Δ his3 trp1 leu2 ura3 mfa2::pFUS1-GFP pADH1-rtTA*	background strain: Allows doxycycline-induction
Hy8y	BY4741r5	*leu2 met15 ura3 pADH1-rtTA pTET07-GFP*	Fig. S2 Measure strength of *pTET07* due to *pADH1-rtTA*
Hy221y	CBHY8DB	*KanMX MATa far1Δ bar1Δ his3 trp1 leu2 pSTE2-GFP*	fig. S3
Hy22y	CB009r5	*HygB far1Δ bar1Δ trp1 leu2 ura3*	Fig. 2C-D,

		pADH1-rtTA *pTET07-MFα1* *pFUS1-GFP*	fig. S4-S7: basic secrete-and-sense strain
Hy222y	CB009r5	*HygB far1Δ bar1Δ his3 trp1 leu2* *pADH1-mCherry* *pADH1-rtTA* *pFUS1-GFP*	Fig. 2C-D, fig. S4-S7: basic sense-only strain
Hy73y	CB008	*KanMX far1Δ his3 trp1 leu2 ura3 ste2Δ*	background strain for *ste2Δ*
Hy74y	CB009	*KanMX far1Δ bar1Δ his3 trp1 leu2 ura3 mfa2::pFUS1-GFP ste2Δ*	background strain for *ste2Δ*
Hy76y	CB009r5	*HygB KanMX far1Δ bar1Δ his3 trp1 leu2 ura3 ste2Δ* *pFUS1-GFP* *pADH1-rtTA*	background strain for *ste2Δ*
Hy86y	Hy76y	*HygB KanMX far1Δ bar1Δ trp1 leu2 ura3 ste2Δ* *pFUS1-GFP* *pADH1-rtTA* *pTET07-MFα1*	background strain for all secrete-and-sense strains with constitutive expression of *STE2*
Hy192y	Hy86y	*HygB KanMX far1Δ bar1Δ trp1 leu2 ste2Δ* *pFUS1-GFP* *pADH1-rtTA* *pTET07-MFα1* *pKEX2-STE2*	Fig. 2E-F
Hy194y	Hy86y	*HygB KanMX far1Δ bar1Δ trp1 leu2 ste2Δ* *pFUS1-GFP* *pADH1-rtTA* *pTET07-MFα1* *pSTE5-STE2*	Fig. 2E-F
Hy196y	Hy86y	*HygB KanMX far1Δ bar1Δ trp1 leu2 ste2Δ* *pFUS1-GFP* *pADH1-rtTA* *pTET07-MFα1* *pGPD1-STE2*	Fig. 2E-F
Hy207y	Hy86y	*HygB KanMX far1Δ bar1Δ leu2 ura3 ste2Δ* *pFUS1-GFP* *pADH1-rtTA* *pTET07-MFα1* *pCYC1-STE2*	Fig. 2E-F
Hy208y	Hy207y	*HygB KanMX far1Δ bar1Δ leu2 ste2Δ* *pFUS1-GFP* *pADH1-rtTA* *pTET07-MFα1* *pCYC1-STE2*	Fig. 2E-F

		pKEX2-STE2	
Hy209y	Hy86y	*HygB KanMX far1Δ bar1Δ leu2 ura3 ste2Δ pFUS1-GFP pADH1-rtTA pTET07-MFα1 pTEF1(m6)-STE2*	Fig. 2E-F
Hy210y	Hy86y	*HygB KanMX far1Δ bar1Δ leu2 ura3 ste2Δ pFUS1-GFP pADH1-rtTA pTET07-MFα1 pTEF1(m7)-STE2*	Fig. 2E-F
Hy211y2	Hy86y	*HygB KanMX far1Δ bar1Δ leu2 ura3 ste2Δ pFUS1-GFP pADH1-rtTA pTET07-MFα1 pTEF1(m10)-STE2*	Fig. 2E-F
Hy215y	Hy86y	*HygB KanMX far1Δ bar1Δ leu2 ura3 ste2Δ pFUS1-GFP pADH1-rtTA pTET07-MFα1 pURA3-STE2*	Fig. 2E-F
Hy228y	Hy76y	*HygB KanMX far1D bar1D his3 trp1 leu2 ste2D pFUS1-GFP pADH1-rtTA pADH1-mCherry*	Background strain
Hy51y	CB008r2	*HygB far1Δ his3 trp1 ura3 pADH1-rtTA* pURA3-GFP	fig. S8:
Hy130y	CB8F1	*HygB far1Δ trp1 leu2 ura3 pFUS1-rtTA pTEF1-GFP*	fig. S8
Hy131y	CB8F1	*HygB far1Δ trp1 leu2 ura3 pFUS1-rtTA pTEF1(m3)-GFP*	fig. S8
Hy132y	CB8F1	*HygB far1Δ trp1 leu2 ura3 pFUS1-rtTA pTEF1(m6)-GFP*	fig. S8
Hy133y	CB8F1	*HygB far1Δ trp1 leu2 ura3 pFUS1-rtTA pTEF1(m7)-GFP*	fig. S8
Hy134y	CB8F1	*HygB far1Δ trp1 leu2 ura3*	fig. S8

		pFUS1-rtTA *pTEF1(m10)-GFP*	
Hy135y	CB8F1	*HygB far1Δ trp1 leu2 ura3* *pFUS1-rtTA* *pKEX2-GFP*	fig. S8
Hy136y	CB8F1	*HygB far1Δ trp1 leu2 ura3* *pFUS1-rtTA* *pSTE5-GFP*	fig. S8
Hy137y	CB8F1	*HygB far1Δ trp1 leu2 ura3* *pFUS1-rtTA* *pGPD1-GFP*	fig. S8
Hy138y	CB8F1	*HygB far1Δ trp1 leu2 ura3* *pFUS1-rtTA* *pCYC1-GFP*	fig. S8
Hy151y	Hy131y	*HygB far1Δ trp1 ura3* *pFUS1-rtTA* *pTEF1(m3)-GFP* *pTEF1(m10)-GFP*	fig. S8
Hy153y	Hy132y	*HygB far1Δ trp1 ura3* *pFUS1-rtTA* *pTEF1(m6)-GFP* *pTEF1(m7)-GFP*	fig. S8
Hy192Sy1	Hy228y	*HygB KanMX far1Δ bar1Δ his3 leu2 ste2Δ* *pFUS1-GFP* *pADH1-rtTA* *pKEX2-STE2* *pADH1-mCherry*	Fig. 2E-F fig. S9
Hy194SyA	Hy194y	*HygB KanMX far1Δ bar1Δ leu2 ste2Δ* *pFUS1-GFP* *pADH1-rtTA* *pSTE5-STE2* *pADH1-mCherry*	Fig. 2E-F fig. S9
Hy196Sy1	Hy228y	*HygB KanMX far1Δ bar1Δ his3 leu2 ste2Δ* *pFUS1-GFP* *pADH1-rtTA* *pGPD1-STE2* *pADH1-mCherry*	Fig. 2E-F fig. S9
Hy207Sy1	Hy228y	*HygB KanMX far1Δ bar1Δ his3 leu2 ste2Δ* *pFUS1-GFP* *pADH1-rtTA* *pCYC1-STE2* *pADH1-mCherry*	Fig. 2E-F fig. S9

Hy208Sy1	Hy207Sy1	*HygB KanMX far1Δ bar1Δ leu2 ste2Δ* *pFUS1-GFP* *pADH1-rtTA* *pCYC1-STE2* *pKEX2-STE2* *pADH1-mCherry*	Fig. 2E-F fig. S9
Hy209Sy1	Hy228y	*HygB KanMX far1Δ bar1Δ his3 leu2 ste2Δ* *pFUS1-GFP* *pADH1-rtTA* *pTEF1(m6)-STE2* *pADH1-mCherry*	Fig. 2E-F fig. S9
Hy210Sy1	Hy228y	*HygB KanMX far1Δ bar1Δ his3 leu2 ste2Δ* *pFUS1-GFP* *pADH1-rtTA* *pTEF1(m7)-STE2* *pADH1-mCherry*	Fig. 2E-F fig. S9
Hy211Sy2	Hy228y	*HygB KanMX far1Δ bar1Δ his3 leu2 ste2Δ* *pFUS1-GFP* *pADH1-rtTA* *pTEF1(m10)-STE2* *pADH1-mCherry*	Fig. 2E-F fig. S9
Hy215Sy1	Hy228y	*HygB KanMX far1Δ bar1Δ his3 leu2 ste2Δ* *pFUS1-GFP* *pADH1-rtTA* *pURA3-STE2* *pADH1-mCherry*	Fig. 2E-F fig. S9
Hy69y	CB8F1	*HygB far1Δ trp1 leu2 ura3* *pFUS1-rtTA* *pTET07-GFP*	background strain
Hy188y	CB8F1DB	*KanMX HygB far1Δ bar1Δ his3 trp1 ura3* *pFUS1-rtTA* *pTET07-GFP*	fig. S10 parent of secrete-and-sense strains with positive feedback
Hy190y	Hy188y	*KanMX HygB far1Δ bar1Δ trp1 ura3* *pFUS1-rtTA* *pTET07-GFP* *pTET07-MFα1*	Figs. 3-4 figs. S11-S13
Hy188-1y1	Hy188y	*KanMX HygB far1Δ bar1Δ his3 trp1* *pFUS1-rtTA* *pTET07-GFP* *pADH1-mCherry*	fig. S13
Hy201y	Hy190y	*KanMX HygB far1Δ bar1Δ trp1* *pFUS1-rtTA* *pTET07-GFP* *pTET07-MFα1*	Fig. 4 fig. S14

		pTEF1(m3)-BAR1	
Hy202y	Hy190y	*KanMX HygB far1Δ bar1Δ trp1* *pFUS1-rtTA* *pTET07-GFP* *pTET07-MFα1* *pTEF1(m7)-BAR1*	Fig. 4 fig. S14
Hy223y	Hy202y	*KanMX HygB far1Δ bar1Δ trp1* *pFUS1-rtTA* *pTET07-GFP* *pTET07-MFα1* *pTEF1(m6)-BAR1* *pTEF1(m7)-BAR1*	Fig. 4 fig. S14
Hy225y	Hy190y	*KanMX HygB far1Δ bar1Δ ura3* *pFUS1-rtTA* *pTET07-GFP* *pTET07-MFα1* *pTEF1(m6)-BAR1*	Fig. 4 fig. S14
Hy226y	Hy201y	*KanMX HygB far1Δ bar1Δ* *pFUS1-rtTA* *pTET07-GFP* *pTET07-MFα1* *pTEF1(m3)-BAR1* *pTEF1(m10)-BAR1*	Fig. 4 fig. S14
Hy218y	Hy190y	*KanMX HygB far1Δ bar1Δ ura3* *pFUS1-rtTA* *pTET07-GFP* *pTET07-MFα1* *pURA3-BAR1*	Fig. 4 fig. S15
Hy219y	Hy190y	*KanMX HygB far1Δ bar1Δ trp1* *pFUS1-rtTA* *pTET07-GFP* *pTET07-MFα1* *pKEX2-BAR1*	Fig. 4 fig. S15
Hy224y	Hy190y	*KanMX HygB far1Δ bar1Δ ura3* *pFUS1-rtTA* *pTET07-GFP* *pTET07-MFα1* *pCYC1-BAR1*	Fig. 4 fig. S15
Hy182y	CB8HYDB	*KanMX MATa far1Δ bar1Δ his3 trp1 leu2* *pBAR1-GFP*	fig. S20
Hy99y	CB8F1	*HygB far1Δ trp1 leu2 ura3* *pFUS1-rtTA* *(pTET07- MFα1)x3* *pBAR1-BAR1*	Background strain

Hy113y	Hy99y	*HygB far1Δ trp1 ura3* *pFUS1-rtTA* *3x(pTET07- MFα1)* *pTET07-GFP* *pBAR1-BAR1*	fig. S23
Hy114y	Hy113y	*HygB far1Δ trp1* *pFUS1-rtTA* *3x(pTET07- MFα1)* *pTET07-GFP* *pBAR1-BAR1* *pKEX2-BAR1*	fig. S23
Hy115y	Hy113y	*HygB far1Δ trp1* *pFUS1-rtTA* *3x(pTET07- MFα1)* *pTET07-GFP* *pBAR1-BAR1* *pSTE5-BAR1*	fig. S23
Hy117y	Hy113y	*HygB far1Δ ura3* *pFUS1-rtTA* *3x(pTET07- MFα1)* *pTET07-GFP* *pBAR1-BAR1* *pCYC1-BAR1*	fig. S23
Hy118y	Hy113y	*HygB far1Δ ura3* *pFUS1-rtTA* *3x(pTET07- MFα1)* *pTET07-GFP* *pBAR1-BAR1* *pURA3-BAR1*	fig. S23
Hy124y	Hy113y	*HygB far1Δ ura3* *pFUS1-rtTA* *3x(pTET07- MFα1)* *pTET07-GFP* *pBAR1-BAR1* *pTEF1(m3)-BAR1*	fig. S23
Hy125y	Hy113y	*HygB far1Δ ura3* *pFUS1-rtTA* *3x(pTET07- MFα1)* *pTET07-GFP* *pBAR1-BAR1* *pTEF1(m6)-BAR1*	fig. S23
Hy126y	Hy113y	*HygB far1Δ ura3* *pFUS1-rtTA* *3x(pTET07- MFα1)* *pTET07-GFP* *pBAR1-BAR1* *pTEF1(m7)-BAR1*	fig. S23
Hy127y	Hy113y	*HygB far1Δ ura3* *pFUS1-rtTA* *3x(pTET07- MFα1)* *pTET07-GFP* *pBAR1-BAR1* *pTEF1(m10)-BAR1*	fig. S23
Hy129y	Hy113y	*HygB far1Δ ura3*	fig. S23

		pFUS1-rtTA *3x(pTET07- MFα1)* *pTET07-GFP* *pBAR1-BAR1* *pTEF1-BAR1*	
Hy141y	Hy124y	*HygB far1Δ* *pFUS1-rtTA* *3x(pTET07- MFα1)* *pTET07-GFP* *pBAR1-BAR1* *pTEF1(m3)-BAR1* *pTEF1(m10)-BAR1*	fig. S23
Hy142y	Hy125y	*HygB far1Δ* *pFUS1-rtTA* *3x(pTET07- MFα1)* *pTET07-GFP* *pBAR1-BAR1* *pTEF1(m6)-BAR1* *pTEF1(m3)-BAR1*	fig. S23
Hy143y	Hy125y	*HygB far1Δ* *pFUS1-rtTA* *3x(pTET07- MFα1)* *pTET07-GFP* *pBAR1-BAR1* *pTEF1(m6)-BAR1* *pTEF1(m7)-BAR1*	fig. S23
Hy144y	Hy125y	*HygB far1Δ* *pFUS1-rtTA* *3x(pTET07- MFα1)* *pTET07-GFP* *pBAR1-BAR1* *pTEF1(m6)-BAR1* *pTEF1(m10)-BAR1*	fig. S23
Hy145y	Hy129y	*HygB far1Δ* *pFUS1-rtTA* *3x(pTET07- MFα1)* *pTET07-GFP* *pBAR1-BAR1* *pTEF1-BAR1* *pTEF1-BAR1*	fig. S23
Hy146y	Hy129y	*HygB far1Δ* *pFUS1-rtTA* *3x(pTET07- MFα1)* *pTET07-GFP* *pBAR1-BAR1* *pTEF1-BAR1* *pTEF1(m3)-BAR1*	fig. S23
Hy147y	Hy129y	*HygB far1Δ* *pFUS1-rtTA* *3x(pTET07- MFα1)* *pTET07-GFP* *pBAR1-BAR1* *pTEF1-BAR1* *pTEF1(m10)-BAR1*	fig. S23

Hy172y	Hy116y	*HygB far1Δ* *pFUS1-rtTA* *3x(pTET07- MFα1)* *pTET07-GFP* *pBAR1-BAR1* *pGPD1-BAR1* *pGPD1-BAR1*	fig. S23
Hy180y	Hy113y	*HygB far1Δ trp1* *pFUS1-rtTA* *3x(pTET07- MFα1)* *pTET07-GFP* *pBAR1-BAR1* *pGPD1-BAR1*	fig. S23

Table S2.

List of integrating plasmids used in constructing the yeast strains listed in Table S1.
These yeast-integrating plasmids integrate into the yeast genome as a single-copy using homologous recombination. This table contains all the plasmids that were used to construct the yeast strains listed in table S1. Importantly, these plasmids enable one to construct a richer set of strains than those listed in table S1 and a richer set of plasmids than listed here because they all share the same pattern: (ApaI) – (Promoter) – (XhoI) – (Gene (ORF)) – (NotI) – (transcription termination sequence of *C. albicans'* ADH1 gene). Thus this modular structure enables swapping of promoters (using one double-digestion with ApaI and XhoI followed by one ligation step). ORF can be swapped with another by one double-digestion with XhoI and NotI-HF followed by one ligation step. To integrate any of these plasmids as a single-copy are integrated into yeast by using pMEI digestion. pMEI digestion cuts all the plasmids to yield two distinct linearized DNA. One contains no homology to any part of yeast and is thus does not integrate into yeast. The other copy, containing the cloning site mentioned above (ApaI – promoter – XhoI- Gene –NotI – transcription termination), has two ends that are homologous to the 5'-UTR and 3'-UTR of one of *S. cerevisiae*'s auxotrophic markers: *HIS3*, *URA3*, *LEU2*, *TRP1*. All of these plasmids were derived from basic plasmids, which are the yeast integrating plasmis that contained no genes or promoters, and only the restrictions sites in the order described above. They are: pNH603, pNH604, pNH605, and pSV606. pNH603 is the basic starting plasmid for *HIS3*, which has 463-bp homology to *S. cerevisiae*'s 5'-UTR of the *S. cerevisiae*'s *HIS3* and has 535-bp homology to *S. cerevisiae's* 3'-UTR of the *S. cerevisiae*'s *HIS3*. It contains as a selection marker *C. glabrata*'s *HIS3* that *S. cerevisiae* can use. pNH604 is the basic starting plasmid for *TRP1*, which has 396-bp homology to *S. cerevisiae*'s 5'-UTR of the *S. cerevisiae*'s *TRP1* and has 353-bp homology to *S. cerevisiae's* 3'-UTR of the *S. cerevisiae*'s *TRP1*. It contains as a selection marker *C. glabrata*'s *TRP1* that *S. cerevisiae* can use. pNH605 is the basic starting plasmid for *LEU2*, which has 646-bp homology to *S. cerevisiae*'s 5'-UTR of the *S. cerevisiae*'s *LEU2* and has 524-bp homology to *S. cerevisiae's* 3'-UTR of the *S. cerevisiae*'s *LEU2*. It contains as a selection marker *C. glabrata*'s *LEU2* that *S. cerevisiae* can use. pSV606 is the basic starting plasmid for *URA*, which has 765-bp homology to *S. cerevisiae*'s 5'-UTR (and partially ORF) of the *S. cerevisiae*'s *URA3* and has 343-bp homology to *S. cerevisiae's* 3'-UTR of the *S. cerevisiae*'s *URA3*. It contains as a selection marker *C. albicans*' *URA3* that *S. cerevisiae* can use. All plasmids are carried in Tg1 or DH5α turbo *E. coli* cells with the AmpR marker (selected by using the antibiotic Carbenicillin).

Plasmid name	Plasmid description
Hy3E	HygB: pADH1-rtTA
Hy4E	HygB: pADH1-tTA
Hy6E1, Hy6E2	pNH603 (HIS3): pTET07 -GFP
Hy7E6	pNH603: (HIS3); pTET07-BAR1
Hy11E2	pNH603 (HIS3): pTET07 -MFα1
Hy12E6, Hy12E611	pNH603 (HIS3): pGal10-MFα1
Hy18E	pNH603(HIS3): pTET07-Bar1
Hy23E	pNH603 (HIS3): pTET07-STE2
Hy58E1	(HygB): pFUS1->rtTA::Msn2ad
Hy61E2	pNH603 (HIS3): (partial pURA3):(pTET07-GFP)

Hy63E1 & E4	pNH603 (HIS3): :(partial pURA3):{pTET07-GFP}x2
Hy64E1 & E2	pNH603 (HIS3): (partial pURA3):(pTET07-MFα1)
Hy65E1	pNH603 (HIS3): (partial pURA3):(pTET07-GFP)x3
Hy67E1; Hy67E5	pSV606 (URA3): pTET07-mCherry
Hy69E1-6	pNH603 (HIS3): (partial pURA3):(pTET-MFα1)x2
Hy73E1; Hy73E2	pSV606 (URA3): pKEX2-BAR1
Hy74E1	pSV606 (URA3): pSTE5-BAR1
Hy75E1,2	pNH604 (TRP1): pGPD1-BAR1
Hy76E1; Hy76E2	pSV606 (URA3): pKEX2-STE2
Hy77E1	pSV606 (URA3): pSTE5-STE2
Hy78E-A & B	pNH604 (TRP1): pGPD1-STE2
Hy79E3	pNH603 (HIS3):(pTET07- MFα1)x3
Hy82E4-6	pNH604 (TRP): pCyc1-Bar1
Hy83E4-6	pNH604 (TRP): pURA3-Bar1
Hy86E1,3	pNH605 (LEU2): pTET07-GFP
Hy89E1-3,5,6,7	pSV606 (URA3): pTET07-BAR1
Hy90E	pNH604 (TRP1): pTEF1(m3)-Bar1
Hy91E1,2	pNH604 (TRP1): pTEF1(m6)-Bar1
Hy92E1,2	pNH604 (TRP1): pTEF1(m7)-Bar1
Hy93E	pNH604 (TRP1): pTEF1(m10)-Bar1
Hy94E	pNH603 (HIS3): pTEF1-GFP
Hy95E	pNH603 (HIS3): pTEF1(m3)-GFP
Hy96E	pNH603 (HIS3): pTEF1(m6)-GFP
Hy97E	pNH603 (HIS3): pTEF1(m7)-GFP
Hy98E	pNH603 (HIS3): pTEF1(m10)-GFP
Hy99E	pNH603 (HIS3): pKEX2-GFP
Hy100E	pNH603 (HIS3): pSTE5-GFP
Hy101E	pNH603 (HIS3): pGPD1-GFP
Hy102E	pNH603 (HIS3): pCYC1-GFP
Hy103E3	pNH604 (TRP1): pTEF1-BAR1
Hy107E1,2	pSV606 (URA): pTEF1-BAR1
Hy108E1,2	pSV606 (URA): pTEF1(m3)-BAR1
Hy109E1,2	pSV606 (URA): pTEF1(m7)-BAR1
Hy110E1,2	pSV606 (URA): pTEF1(m10)-BAR1
Hy111E1,2	pNH605 (LEU2): pTEF1-GFP
Hy112E1,2	pNH605 (LEU2): pTEF1(m3)-GFP
Hy113E1,2	pNH605 (LEU2): pTEF1(m6)-GFP
Hy114E1,2	pNH605 (LEU2): pTEF1(m10)-GFP
Hy115E1,2	pSV606 (URA3): pADH1-BAR1

Hy116E3,5	pSV606 (URA3): pGPD1-BAR1
Hy117E1,2	pSV606 (URA3): pADH1-GFP
Hy118E2	pSV606 (URA3): pADH1-mCherry
Hy119E1,2	pSV606 (URA3): pBAR1(1 PRE)-GFP
Hy120E 1,2	pSV606 (URA3): pBAR1(2 PRE)-GFP
Hy121E 1	pSV606 (URA3): pBAR1(1 PRE)-mCherry
Hy122E 1,2	pSV606 (URA3): pBAR1(2 PRE)-mCherry
Hy123E	pNH604(TRP): pTEF1-STE2
Hy124E	pNH604(TRP): pTEF1(m3)-STE2
Hy125E-A, B	pNH604(TRP): pTEF1(m6)-STE2
Hy126E-A, B	pNH604(TRP): pTEF1(m7)-STE2
Hy127E-A, -B	pNH604(TRP): pTEF1(m10)-STE2
Hy128E	pNH604(TRP): pGPD1-STE2
Hy129E	pNH604(TRP): pADH1-STE2
Hy130E	pNH604(TRP): pCYC1-STE2
Hy131E	pNH604(TRP): pSTE5-STE2
Hy132E	pNH604(TRP): pKEX2-STE2
Hy133E-A	pNH604(TRP): pURA3-STE2
Hy137E1	pNH606(URA): pSTE2-GFP
pNH603	HIS3 selection marker, basic yeast integrating plasmid
pNH604	TRP1 selection marker, basic yeast integrating plasmid
pNH605	LEU2 selection marker, basic yeast integrating plasmid
pSV606	URA3 selection marker, basic yeast integrating plasmid

References

101. E. Nevoigt *et al*. Engineering of promoter replacement cassettes for fine-tuning of gene expression in Saccharomyces cerevisiae, *App. Env. Microbiol.* **72** (8), 5266-5273 (2006). doi:10.1128/AEM.00530-06 PMID 16885275

102. H. Alper, C. Fischer, E. Nevoigt, G. Stephanopoulos, Tuning genetic control through promoter engineering. *Proc. Natl. Acad. Sci. USA* **102** (36), 12678-12683 (2005). doi:10.1073/pnas.0504604102 PMID 16123130